NASA TN D-1496

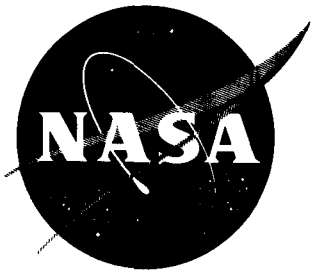

TECHNICAL NOTE

D-1496

LANDING CHARACTERISTICS OF A WINGED REENTRY VEHICLE WITH ALL-SKID LANDING GEAR HAVING YIELDING-METAL SHOCK ABSORBERS

By Ulysse J. Blanchard

Langley Research Center
Langley Station, Hampton, Va.

NATIONAL AERONAUTICS AND SPACE ADMINISTRATION
WASHINGTON December 1962

NATIONAL AERONAUTICS AND SPACE ADMINISTRATION

TECHNICAL NOTE D-1496

LANDING CHARACTERISTICS OF A WINGED REENTRY VEHICLE WITH ALL-SKID LANDING GEAR HAVING YIELDING-METAL SHOCK ABSORBERS

By Ulysse J. Blanchard

SUMMARY

An experimental investigation has been made of the landing characteristics of a 1/10-scale dynamic model of a winged reentry vehicle having an all-skid landing gear and replaceable strut energy straps for dissipating landing energy. The gear consisted of twin main skids near the wing trailing edge and a single "dishpan" nose skid. The landing tests were made by catapulting a free model onto a hard-surface runway. Landing motions and acceleration data were obtained for a range of initial sinking speeds, landing attitudes, and gear configurations. A few slideout (landing run) stability tests were also made for yawed touchdown conditions.

Slideout characteristics and directional stability of the vehicle were good in the speed range of the investigation for ratios of main-skid to nose-skid coefficient of friction of approximately 1.0 to 3.0 and initial roll and yaw angles up to 15°. Maximum normal landing accelerations were approximately 3g at the center of gravity and 5g at the nose gear for the range of landing conditions and gear geometry. Touchdown pitch and yaw attitude, landing speed, and sinking speed had no effect on maximum accelerations as expected for yielding-metal shock absorbers (energy straps) with sufficient working stroke. Rolled touchdowns or the use of auxiliary skid energy straps resulted in reduced accelerations at initial main-gear impact (halved shock-absorber force) but did not affect nose-gear impact accelerations. In general, moving the nose gear forward or reducing initial strut sweepback increased accelerations at first nose-gear impact.

INTRODUCTION

The evaluation and development of efficient spacecraft recovery systems incorporating basic simplicity, reliability, and environmental adaptability are of continuing interest. Since the take-off mode (rocket launched) and anticipated infrequent landings of spacecraft allow the use of a "one-shot" type landing gear, simplicity and reliability are enhanced. Most winged spacecraft (fixed or variable geometry) give low touchdown sinking speeds by means of the conventional flared landing. Such vehicles have maneuver and range capabilities

permitting landings on prepared or existing runways, a feature contributing to optimization of landing systems. High horizontal speeds or touchdown-point errors generally associated with unpowered landings, however, make it desirable to reduce slideout (landing run) distance and maintain directional control with minimum reliance on special apparatus such as steering mechanisms, drogue parachutes, or runway arresting gear. Also, the complexities encountered in adaptir conventional oleo shock-absorption devices or braking devices to reentry enviror ment are undesirable.

Various landing-gear concepts involving skids or yielding-metal shock absorbers have been proposed for winged reentry vehicles and reported in references 1, 2, and 3. An additional system employs an all-skid tricycle landing gear which provides inherent braking force, directional stability, and nonviscou shock absorbers. Landing-impact energy in this case is dissipated by yielding a replaceable energy strap in tension with a pivot and strut arrangement which als supports the vehicle during the landing slideout on the skids. The energy strap is readily adaptable to high temperatures and, since energy is absorbed by yielding a ductile metal, little energy is stored; thus, rebound is minimized. Directional stability during slideout is obtained by providing differential coef ficient of friction between the nose- and main-gear skids.

This report will discuss the results of an investigation of the landing-impact and slideout characteristics of a winged reentry vehicle employing the proposed landing gear. Impact acceleration and behavior were determined with a free dynamic model landing on a hard-surface runway. A range of initial sinking speeds and landing attitudes, several gear configurations, and the effect of an auxiliary shock absorber were investigated.

DESCRIPTION OF MODEL

The general arrangement of the 1/10-scale dynamic model is shown in figure Photographs of the model with the basic landing gear are shown as figure 2. Details of the basic and modified landing-gear configurations are shown in figures 3 and 4, respectively. The addition of auxiliary skid energy straps to th modified gear is illustrated in figure 5. Full-scale and model-scale relationships applicable to these tests are given in table I. Pertinent model and full scale dimensions are given in table II.

The model had a flat-plate delta-planform wing (73° leading-edge sweepback and 5° dihedral) which was constructed of balsa and hardwood covered with a thi plastic-impregnated fiber-glass skin. The fuselage was a shell (fiber glass, plastic, and foamed plastic) reinforced internally by longitudinal bulkheads. The fuselage unit was bonded to the upper surface of the wing in order to provi model rigidity. The model launching brackets, vertical tails, and landing-gear components were made of aluminum.

The basic landing gear (figs. 1, 2, and 3) was a tricycle arrangement consisting of a pair of main-gear skids located near the wing trailing edge and a nose-gear skid located well forward of the center of gravity. A circular

"dishpan" nose skid was used to minimize destabilizing side forces (edge effect) at the nose during yawed slideout conditions. In order to facilitate installation and servicing, the model landing gears (fig. 3) were constructed as removable assemblies (attaching channel, pivoted strut, skid, and strut energy strap) which were attached to the wing lower surface at the desired location.

The modified landing gear, resulting from further structural and storing considerations by the prototype designer, employed changes in strut lengths and sweepback angles (fig. 4) and nose-gear location (fig. 1). Additional stroke for absorbing some of the initial landing energy was provided by holding the skid in a nose-up position with an auxiliary energy strap (fig. 5) until ground contact after which rotation of the skid elongated the auxiliary strap.

The model energy straps were made of commercially pure nickel wire ("A" Nickel), a high-elongation metal which retains its mechanical properties at high temperatures. This is one of the metals being considered for prototype application. The nickel wire was used in an annealed condition for these tests. Landing loads imposed on the gear strut were absorbed in tension by the energy strap. The load exceeded the yield strength of the strap and it elongated during the strut stroke. Stress-strain characteristics of a sample of the model energy-strap material are shown in figure 6 for strain rates (2 and 1,300 in./in./min) which are inclusive of values for model and prototype landings (approximately 300 and 100 in./in./min, respectively). The stress-strain curve of an "A" Nickel specimen at a much lower strain rate (0.100 in./in./min) is also shown. Maximum stress was about the same for all strain rates shown resulting in similar model and prototype gear-force characteristics. Therefore, scaling requirements were satisfied by using the prototype energy-strap material for the model tests and scaling the cross-sectional area of the model straps by the factor λ^3 (table I). Typical force characteristics obtained during component tests of the model landing-gear assemblies of the modified gear are shown in figure 7. Gear forces for the basic gear would be similar.

The contemplated range of full-scale friction coefficients (about 0.2 to 0.5) discussed in reference 4 were obtained by surfacing the model skids with appropriate materials. The friction coefficients of the materials were determined from static component tests in which a rotating plywood disk (simulating model test runway surface) was used to determine the friction values shown in figure 8 at speeds corresponding to model test speeds. The coefficient of friction of cork exhibited a large increase with increase in speed. For the purpose of this test and in this report an average value of 0.7 was used for cork.

APPARATUS AND PROCEDURE

The investigation was conducted by launching the model as a free body by use of the monorail apparatus of the Langley impacting structures facility. The model is shown on the monorail launching carriage in figure 9(a). The elevons were set for trimmed flight at the launching attitude and the model maintained approximately this attitude during free glide onto the runway shown in figure 9(b). The runway was constructed of heavy wood decking covered with 1/2-inch plywood

and supported just above the water surface on adjustable steel scaffolding mounted on the bottom of a tank of water. The landing surface was 8 feet wide and approximately 100 feet long with the end sloped into the water. When the model ran beyond the length of the runway provided, it was arrested by the water A brief outline of the test conditions investigated is shown in table III.

Landing Impacts

The orientation of acceleration axes, force directions, and attitude during principal landing impacts are shown in figure 10. Landings were made at touchdown pitch attitudes of 5° to 15°, landing speeds of 105 to 170 knots, and sinki speeds (vertical velocity) of 4 to 12 feet per second (all values converted to full scale). During the landings, most touchdowns occurred with initial roll attitude and in some cases with yaw attitude. The initial sweepback angle of th nose-gear strut was varied from 6° to 36° and three longitudinal locations of th nose gear were also investigated (fig. 1). The forward and intermediate locatio placed the nose gear at a distance from the center of gravity greater than the pitch radius of gyration of the test vehicle (table II). The aft location was less than the radius of gyration. Auxiliary main- and nose-skid energy straps having 50 and 20 percent of strut-strap cross-sectional area, respectively, were briefly tested. Landings were made at a model weight corresponding to a full-scale weight of 8,000 pounds with the basic and 8,500 pounds with the modified gear. The ratio of main-skid to nose-skid coefficient of friction was approximately 2.0 for leather and Teflon used for all landing-impact tests. The same size strut energy straps were used for all landing-impact tests (table II).

Impact accelerations were measured by strain-gage accelerometers rigidly mounted to the model structure. Normal acceleration at the center of gravity wa measured with a 20g accelerometer during landings with the basic gear. With the modified gear, normal acceleration was measured at the gear locations as well as at the center of gravity. Acceleration at the main-gear location was measured with a 15g accelerometer and at the intermediate nose-gear location (fig. 1) wit a 20g accelerometer. Angular acceleration about the center of gravity for all landings (basic and modified gear) was measured with a pair of matched 50g accel erometers. The natural frequency was about 180 cycles per second for the 15g and 20g accelerometers and about 310 cycles per second for the 50g accelerometer The accelerometers were damped to 65 percent of critical damping. The response of the recording galvanometers was flat to about 190 cycles per second for the 15g accelerometer and to about 135 cycles per second for the 20g and 50g accelerometers. A trailing cable, supported by an overhead guide wire, was used to transmit accelerometer signals to an oscillograph recorder. Initial impact poin on the runway were obtained by coating the skids with marking chalk. Measuremen of total gear stroke were made by determining angular displacement of the struts after each landing. Motion-picture and sequence cameras located at the side of the tank and at the end of the runway recorded general behavior during landing-impact tests.

Slideout Characteristics

Although slideout behavior was observed during landing-impact tests, additional directional-stability tests were conducted by launching the model at predetermined yaw attitudes (up to 15°) and 0° pitch and roll just clear of the runway, approximately zero sinking speed, for several ratios of main- to nose-skid coefficient of friction. The ratio of main- to nose-skid coefficient of friction was varied from approximately 0.4 to 3.0 during the slideout stability tests by using combinations of skid surface materials; Teflon, leather, aluminum, and cork. At a launch speed corresponding to full-scale landing speed (105 knots or greater) the model overran the end of the runway before completing the slideout. In order to study low-speed behavior and termination of slideout it was necessary to launch the model at a lower speed (75 knots). The tests were conducted with no cross wind. The camera setup used for landing-impact tests was also used for the slideout tests.

RESULTS AND DISCUSSION

A motion-picture film supplement of typical landing-impact and slideout stability tests is available on loan from the NASA. A request card and a description of the film will be found at the back of this paper, on the page immediately preceding the abstract pages. All data presented are converted to full-scale values by use of the scale relations given in table I. The lines drawn through the impact acceleration data are calculated values.

Landing Impacts

Sequence photographs of typical landings of the model on the runway surface are shown in figure 11. The general behavior was very similar for all landings and was characterized by approach at angle of attack, touchdown impact on the main gear, angular rotation to nose-gear impact, and the slideout. During the landings many asymmetric initial main-gear impacts occurred and the longitudinal distances between initial runway contact and subsequent gear contacts obtained for a sample of 46 landings are plotted in figure 12. The data show that the degree of roll varied over a wide range. In general, roll and yaw attitudes of up to 15° were experienced. Typical pitch-acceleration time histories during the significant landing impacts are shown in figure 13. The main skids contacted initially (first main-gear impact) at which time touchdown sinking-speed energy and friction force at the main gear were absorbed by the energy straps and a rotational impulse (nose down) was imparted to the vehicle. The resulting energy in the system (vertical and rotational) was then absorbed during first nose-gear impact by both the nose- and main-gear energy straps (fig. 13(b)). Energy due to horizontal landing speed was largely dissipated by skid-friction forces during the slideout.

Effect of touchdown sinking speed.- The effect of initial (touchdown) sinking speed on landing-impact accelerations is shown in figures 14 and 15. Maximum normal and angular accelerations at the center of gravity obtained during

landings with the basic gear at the forward location are shown in figure 14 plotted against initial sinking speed. Maximum accelerations obtained at the gear stations during landings with the modified gear and the intermediate nose-gear location are shown in figure 15 for a range of sinking speeds. In each case (center of gravity and gear station) maximum accelerations were essentially constant over the entire sinking-speed range as expected for yielding-metal (constant force) shock absorbers having sufficient working stroke.

Effect of touchdown attitude.- Maximum accelerations obtained during landings at various touchdown pitch attitudes with the modified gear are shown in figure 16. Data for first main-gear impacts obtained during landings with the modified gear, excluding data obtained with auxiliary skid energy straps, are plotted in figure 16(a) against touchdown pitch attitude. Gear geometry was constant for a given touchdown pitch attitude and acceleration was constant as expected. A small change in acceleration resulted with change in touchdown pitch attitude due to the associated change in initial gear geometry with respect to the runway. The solid lines in figure 16(a) are for symmetrical touchdown landings (no roll). The dashed lines are for rolled touchdowns which gave about one-half the initial gear force or acceleration of the symmetrical landings. First nose-gear impact accelerations are shown in figure 16(b). The nose-gear geometry and consequently the gear-reaction force was essentially unchanged by initial touchdown conditions. The data of figure 16 show that horizontal landing speed had no significant effect on accelerations since the landing speed varied from 110 to 170 knots over the range of pitch attitudes tested (5° to 15°).

Effect of nose-strut sweepback.- The maximum accelerations obtained at first nose-gear impact with various initial nose-gear strut sweepback angles are shown in figure 17. Increasing sweepback angle generally reduced accelerations. This reduction is because of the change in geometry (increased mechanical advantage) which reduced the reaction force at the nose gear. Normal accelerations at the nose gear and at the center of gravity were reduced from approximately 5g to 3g and 3g to 2g, respectively, by increasing sweepback from 6° to 36°. Typical fairings of traces of normal accelerations obtained at first nose-gear impact for the various initial nose-gear strut sweepback angles are shown in figure 18. High-frequency model vibrations were excited at impact. The recorded acceleration traces (fig. 18) show a sharp initial acceleration peak (short duration) followed by a lower-magnitude main impulse representing the principal gear-reaction force. This is particularly characteristic of the small initial strut sweepback angles. Only the faired values of the principal gear-reaction accelerations are plotted in figure 17. The gear force characteristics, without skid friction component, shown in figure 7 also indicate a peak starting force for the nose gear at an initial sweepback angle of 15°. Although skid-friction forces during landing would tend to minimize this peak, initial strut sweepback angles of 15° or greater would be advantageous in that peak starting loads at impact are avoided.

Effect of nose-gear location.- The maximum accelerations obtained at first nose-gear impact for three longitudinal nose-gear locations and two initial nose gear strut sweepback angles are shown in figure 19. Normal accelerations at the nose gear increased from approximately $3\frac{1}{2}$g to 5g and angular accelerations

increased from approximately 6 to 15 radians/sec^2 as the gear was moved forward. Normal accelerations at the center of gravity were constant for all locations since the total normal reaction force was unchanged. The increase in normal acceleration at the nose gear with forward movement of the gear resulted from increased normal component due to angular acceleration. The vehicle radius of gyration and the center-of-percussion location for the nose gear relative to the present main-gear location are shown in figure 19. Locating the nose gear near the center of percussion would be desirable from the standpoint of keeping the amount of energy to be absorbed by both gears fairly low (ref. 5). The aft nose-gear location of the present tests (less than radius of gyration and center of percussion) appeared to be a limit since this location, with 36° initial strut sweepback angle shown in figure 19(b), resulted in the main gear being essentially unloaded during nose-gear impact, that is, all load on nose gear. This characteristic is best illustrated by comparing the trace of normal acceleration at the main gear during nose-gear impact shown in figure 20 with the same event in figure 13(b).

Effect of auxiliary energy strap.- Maximum accelerations at first main- and nose-gear impacts obtained during landings with auxiliary skid energy straps installed are shown in figure 21 for various initial strut sweepback angles. The energy straps used on the main skids (which were 50 percent as large as the strut-strap cross-sectional area) reduced maximum normal acceleration at first main-gear impact about 50 percent (fig. 21(a)). The reduction in acceleration was the same as that for an initially rolled impact on one gear (dashed line, fig. 16(a)). It was observed that most of the energy of initial main-gear impact was dissipated by the skid energy straps; thereby, very little of the available strut stroke was used. The nose-skid energy strap (which was 20 percent as large as the strut-strap cross-sectional area) was not as effective and no significant change in accelerations resulted.

Slideout Characteristics

Landing slideout.- During landing-impact tests (15° pitch attitude) many landings occurred with various degrees of roll and yaw. The rolled landings caused asymmetric strut deflections which resulted in slideouts with the vehicle canted over several degrees. In one or two cases, one of the main-gear struts was fully deflected (due to energy-strap failure) causing a severe roll condition during slideout. Directional stability was good during slideouts under these rolled conditions. During yawed landings, the vehicle returned to approximately unyawed heading during the time between first main-gear and first nose-gear contact due to high skid-friction forces aft and the inherent aerodynamic stability. An extreme case was that of the vehicle landing at very high roll and yaw attitude on one main gear, rolling over onto the low wing, then righting itself after nose-gear impact to continue a stable slideout.

Slideout stability.- The slideout stability tests resulted in touchdowns with all gear simultaneously contacting the runway at approximately the desired yaw attitude (up to 15°). Typical slideouts with the intermediate nose-gear location obtained with ratios of main- to nose-skid coefficient of friction ranging from approximately 2.0 (lower coefficient at nose) to 0.4 (higher

coefficient at nose) during tests at 10° initial yaw and at two launch speeds ar shown in figures 22 and 23. The model was directionally stable over the entire speed range at a coefficient-of-friction ratio of 1.0 to 3.0 (maximum investigated) for initial yaw angles up to 15°. At friction ratios less than 1.0 insta bility occurred at low speeds. At high speeds aerodynamic effects provided some directional stability (fig. 22(c)). The instabilities that occurred did not appear disastrous, and in most cases the vehicle remained within a 40-foot runwa width.

CONCLUSIONS

Results of the dynamic-model investigation indicate that hard-surface landi characteristics of a winged-reentry vehicle having an all-skid tricycle landing gear and replaceable yielding-metal shock absorbers (energy straps) were good fc a wide range of landing conditions. The principal conclusions indicated by this investigation are as follows:

1. Maximum normal accelerations obtained during landings were approximately 3g at the center of gravity and 5g at the nose gear. Maximum angular accelerati was approximately 15 radians/sec^2. Maximum landing acceleration always occurred at first nose-gear impact.

2. The landing gear was insensitive to impact velocity during landings ove a range of initial sinking speeds of 4 to 12 feet per second, touchdown pitch attitudes of 5° to 15°, and landing speeds of 105 to 170 knots. Maximum accelerations remained constant when there was sufficient gear stroke available to prevent bottoming.

3. Rolled touchdown or the application of auxiliary skid energy straps reduced accelerations during the first main-gear impact.

4. With a given energy-strap configuration, moving the nose gear forward o reducing initial strut sweepback generally increased accelerations at first nos gear impact.

5. A satisfactory nose-gear geometry would be obtained by locating the nos gear near the center of percussion with a strut sweepback angle of 15° or great

6. Slideout characteristics and directional stability were good in the spe range of the investigation for ratios of main- to nose-skid coefficient of fric tion of approximately 1.0 to 3.0 and initial roll and yaw angles up to 15°.

Langley Research Center,
National Aeronautics and Space Administration,
Langley Station, Hampton, Va., August 14, 1962.

REFERENCES

1. Blanchard, Ulysse J.: Landing-Impact Characteristics of Load-Alleviating Struts on a Model of a Winged Space Vehicle. NASA TN D-541, 1960.

2. Blanchard, Ulysse J.: Landing Characteristics of a Lenticular-Shaped Reentry Vehicle. NASA TN D-940, 1961.

3. McKay, James M., and Kordes, Eldon E.: Landing Loads and Dynamics of the X-15 Airplane. NASA TM X-639, 1962.

4. Dreher, Robert C., and Batterson, Sidney A.: Coefficients of Friction and Wear Characteristics for Skids Made of Various Metals on Concrete, Asphalt, and Lakebed Surfaces. NASA TN D-999, 1962.

5. Houbolt, John C., and Batterson, Sidney A.: Some Landing Studies Pertinent to Glider-Reentry Vehicles. NASA TN D-448, 1960.

TABLE I.- SCALE RELATIONSHIPS

[λ = Scale of model]

Quantity	Full scale	Scale factor	Model
Dynamic model:			
Length	l	λ	λl
Area	A	λ^2	$\lambda^2 A$
Weight	W	λ^3	$\lambda^3 W$
Moment of inertia . . .	I	λ^5	$\lambda^5 I$
Time	t	$\sqrt{\lambda}$	$\sqrt{\lambda}$ t
Speed	V	$\sqrt{\lambda}$	$\sqrt{\lambda}$ V
Linear acceleration . .	a	1	a
Angular acceleration . .	α	λ^{-1}	$\lambda^{-1}\alpha$
Force	F	λ^3	$\lambda^3 F$
Energy strap:			
Unit stress	σ	1	σ
Cross-sectional area[1]. .	A_s	λ^3	$\lambda^3 A_s$
Force	F_s	λ^3	$\lambda^3 F_s$

[1]For dynamic similarity it is convenient to keep linear accelerations 1:1 for model and full scale. Since the mass varies as the cube of the scale factor (λ^3) all applied forces must be varied by the same factor. A geometrically scal energy strap would vary as λ^2; therefore, it is necessary to distort the cross-sectional area of the strap and vary it as λ^3.

TABLE II.- PERTINENT DIMENSIONS OF THE VEHICLE

	1/10-scale model	Full scale
General:		
Gross weight, lb	8.0	8,000
Moment of inertia (approximate):		
Roll, slug-ft^2	0.037	3,700
Pitch, slug-ft^2	0.167	16,700
Yaw, slug-ft^2	0.189	18,900
Pitch radius of gyration, ft	0.821	8.21
Gross weight, lb	8.5	8,500
Moment of inertia (approximate):		
Roll, slug-ft^2	0.043	4,300
Pitch, slug-ft^2	0.185	18,500
Yaw, slug-ft^2	0.230	23,000
Pitch radius of gyration, ft	0.838	8.38
Wing:		
Root chord, ft	2.96	29.55
Span, ft	1.64	16.35
Mean aerodynamic chord, $\bar{c}$, ft	2.23	22.3
Area, sq ft	3.3	330
Loading, lb/sq ft	2.42	24.2
Center of gravity, percent $\bar{c}$	43	43
Tail surfaces:		
Elevon area (each), sq ft	0.184	18.4
Vertical-fin area (each), sq ft	0.298	29.8
Main landing gear (2):		
Distance from center of gravity to strut pivot, ft	0.855	8.55
Strut energy strap (each gear):		
Cross-sectional area, sq ft	1.63×10^{-6}	1.63×10^{-3}
Length, ft	0.33	3.33
Nose gear:		
Distance from center of gravity to strut pivot for -		
Forward location, ft	1.333	13.33
Intermediate location, ft	1.042	10.42
Aft location, ft	0.750	7.50
Strut energy strap:		
Cross-sectional area, sq ft	8.72×10^{-6}	8.72×10^{-3}
Length, ft	0.25	2.50

TABLE III.- TEST CONDITIONS

Test category	Landing-gear configuration	Test data	Test parameter
Landing impact	Basic	Normal acceleration at center of gravity Angular acceleration	Sinking speed
	Modified	Normal acceleration at center of gravity Normal acceleration at gear Angular acceleration	Sinking speed Touchdown attitude Nose-strut sweepback Nose-gear location Auxiliary energy strap
Slideout	Basic	Slideout behavior during landing-impact tests	Sinking speed
	Modified		Sinking speed Touchdown attitude Nose-strut sweepback Nose-gear location Auxiliary energy strap
	Modified	Slideout stability for yawed touchdown	Ratio of main- to nose-skid coefficient of friction

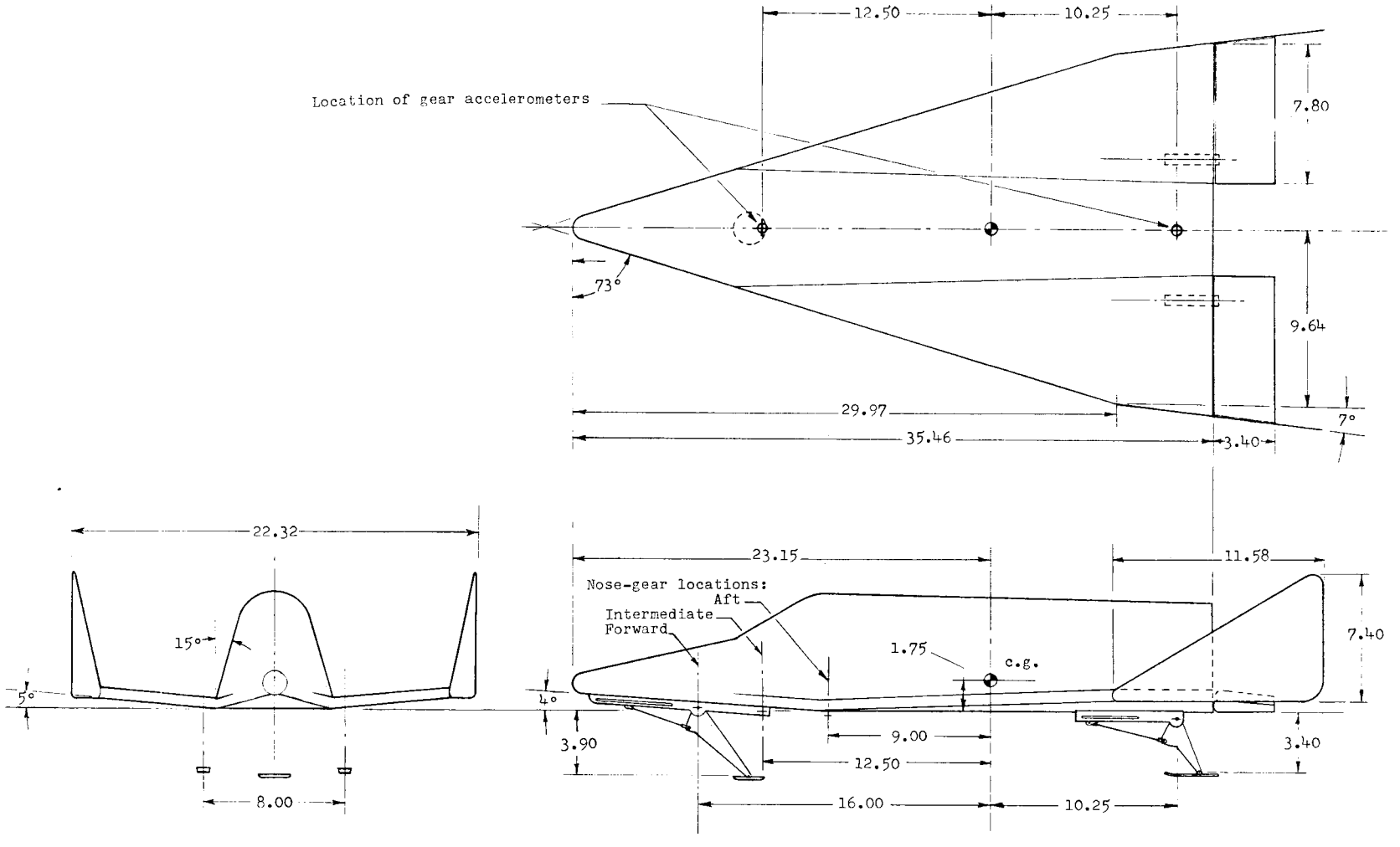

Figure 1.- General arrangement of 1/10-scale dynamic model. All dimensions are in inches.

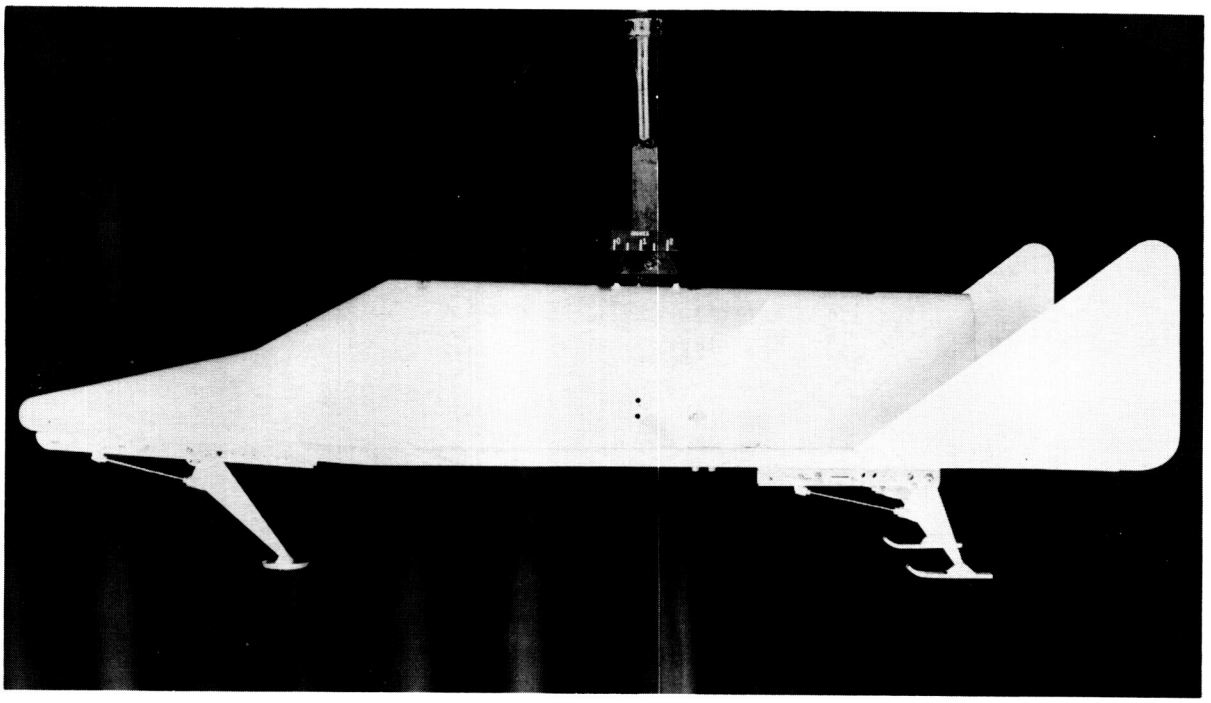

(a) Side view. L-60-3855

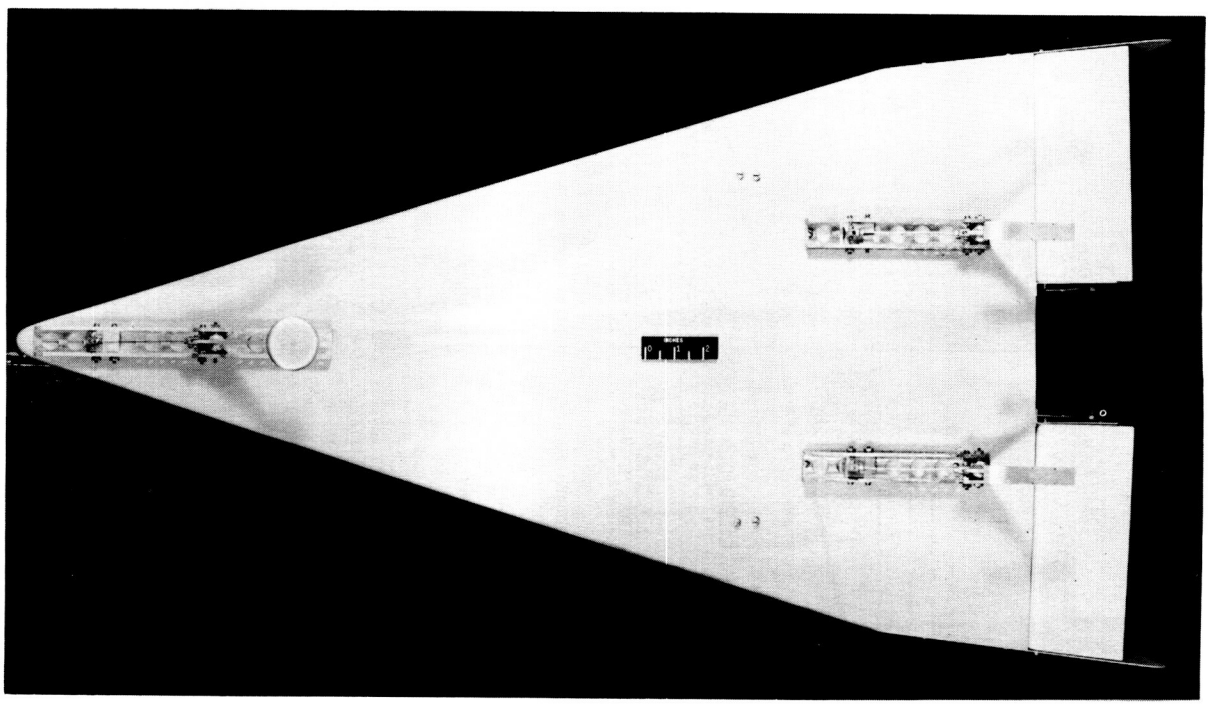

(b) Bottom view. L-60-3861

Figure 2.- Photographs of model.

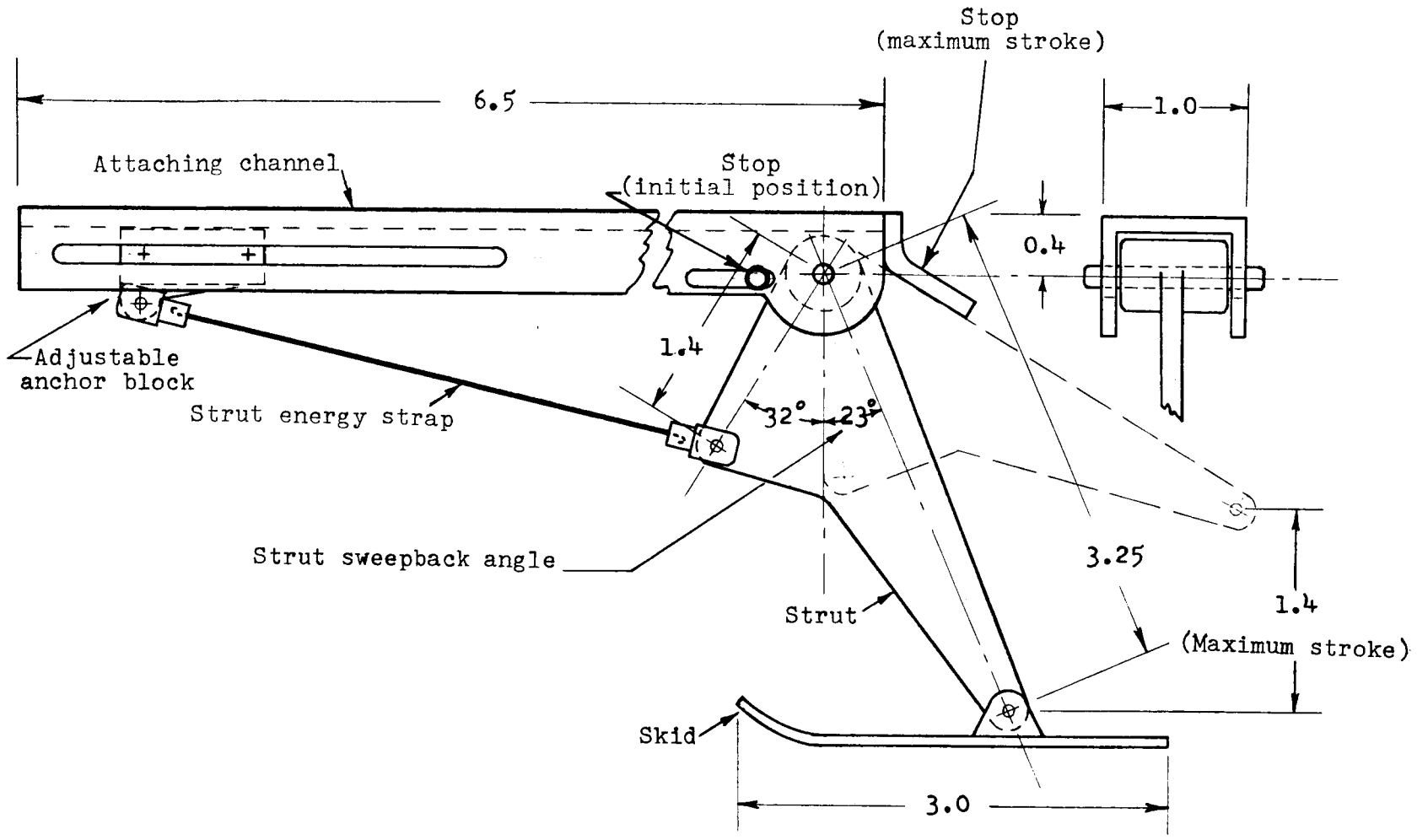

(a) Main gear.

Figure 3.- Details of basic model landing-gear assemblies. All dimensions are in inches.

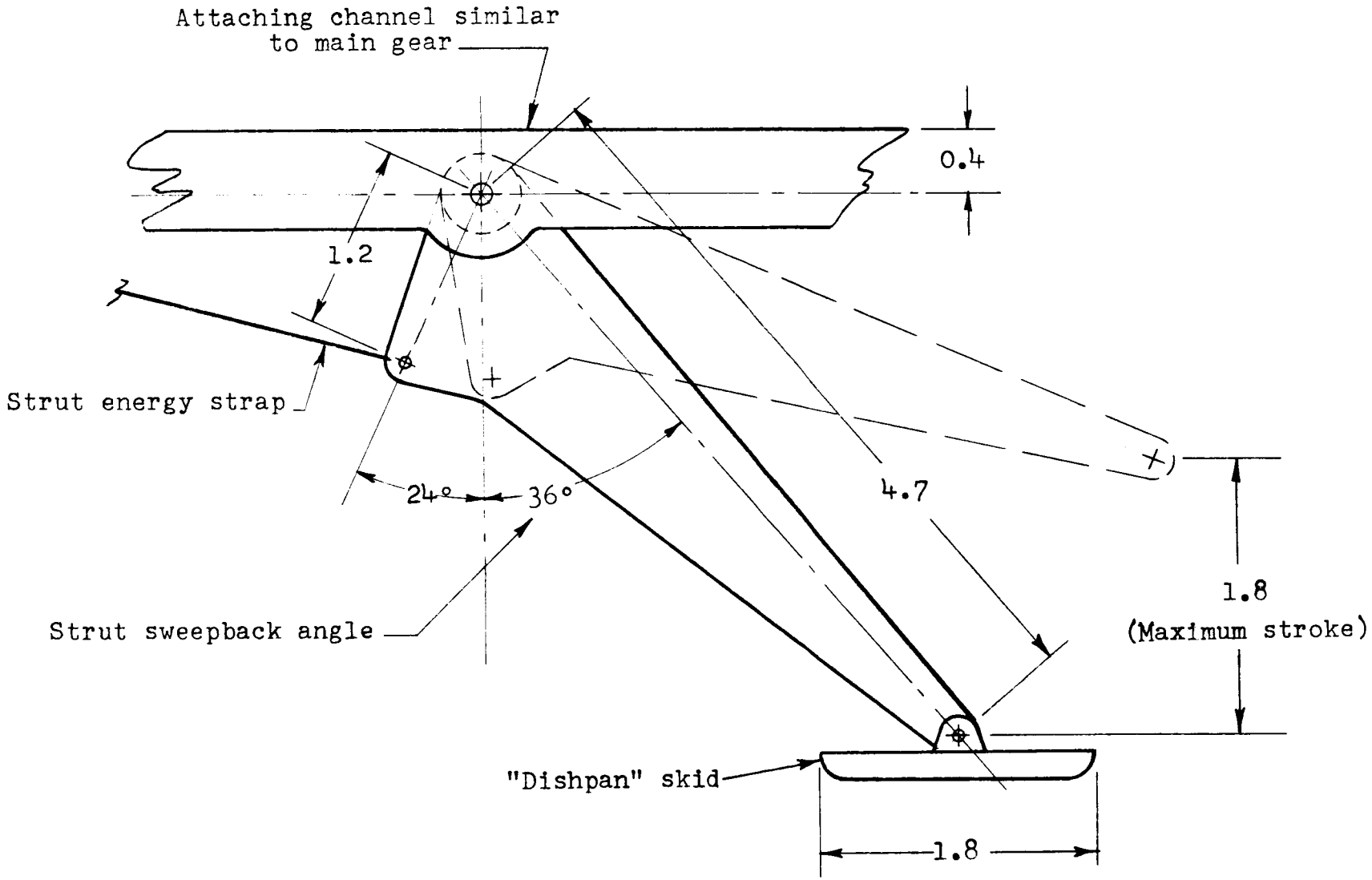

(b) Nose gear.

Figure 3.- Concluded.

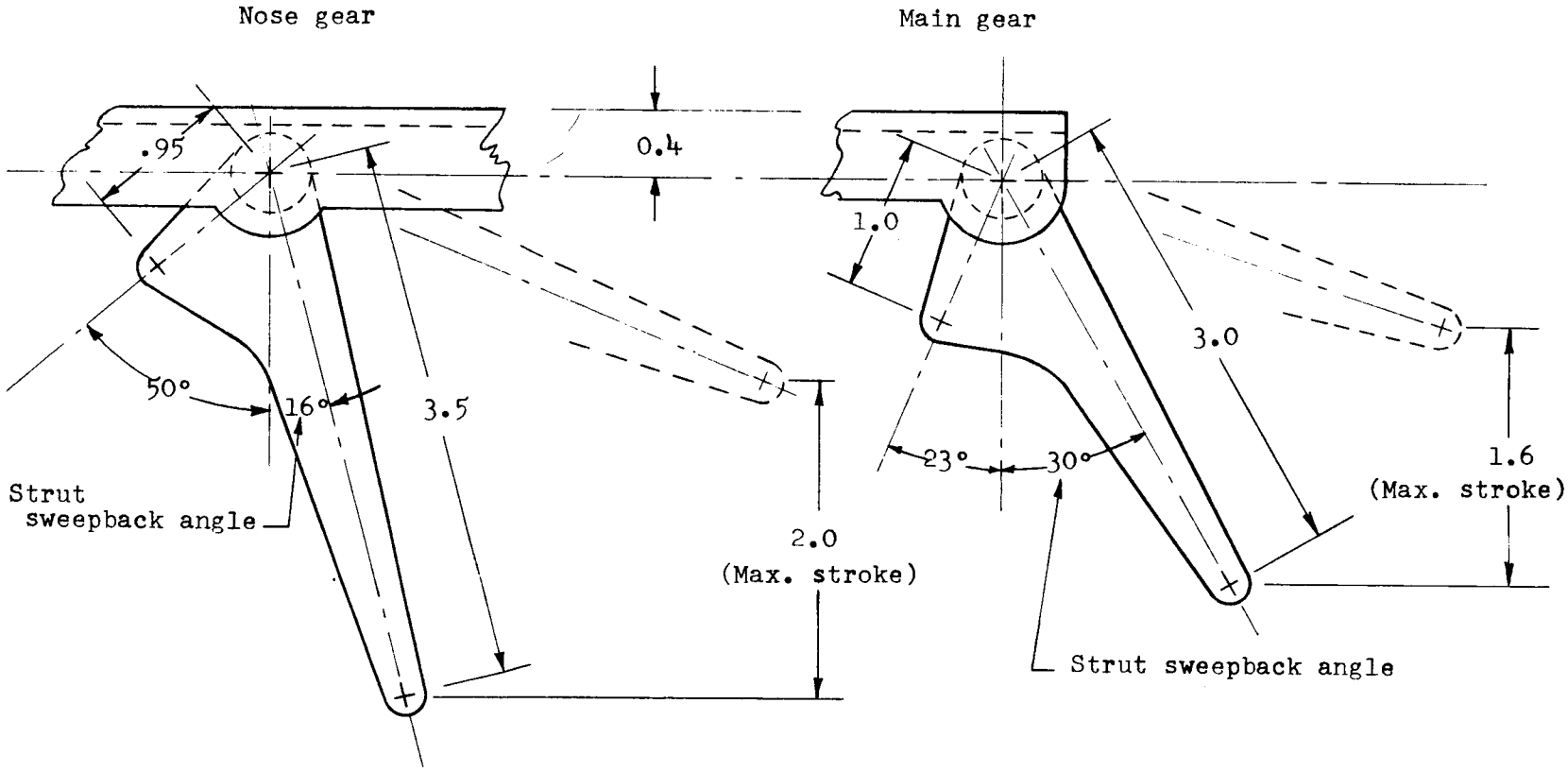

Figure 4.- Details of modified model landing-gear struts. All dimensions are in inches.

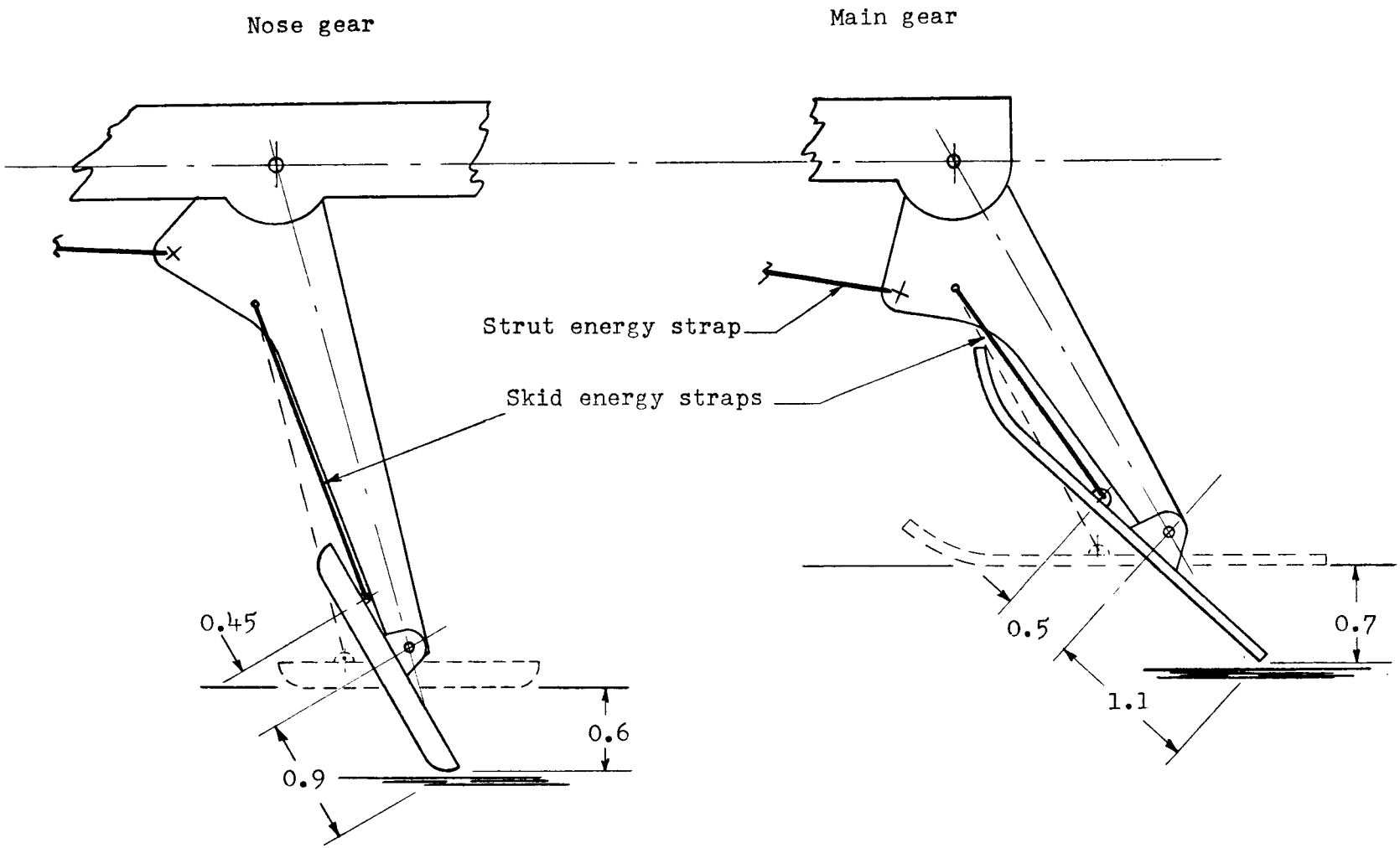

Figure 5.- Modified model landing gear with auxiliary energy straps. All dimensions are in inches.

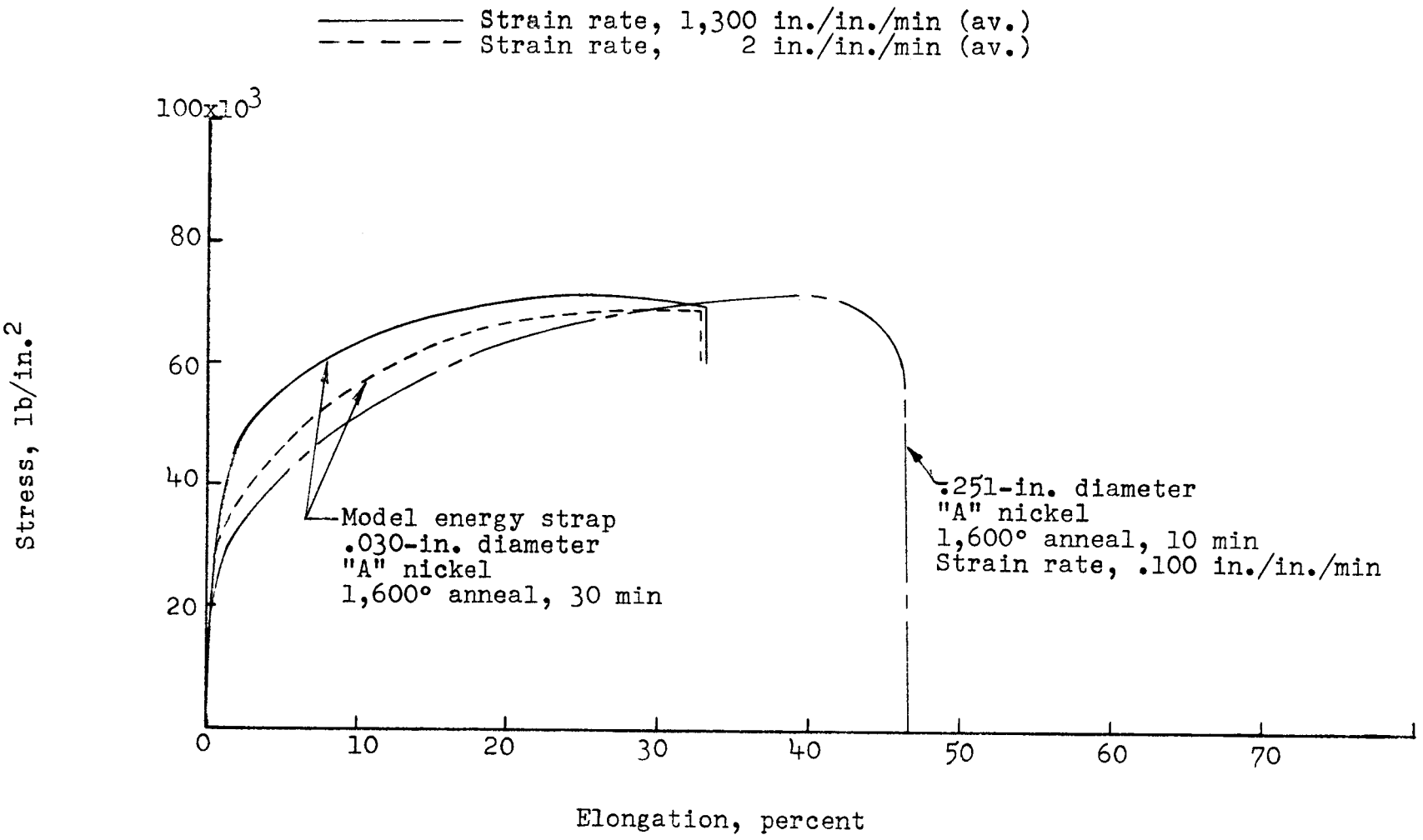

Figure 6.- Stress-strain characteristics of model landing-gear energy strap showing effect of impact loading and strain rate.

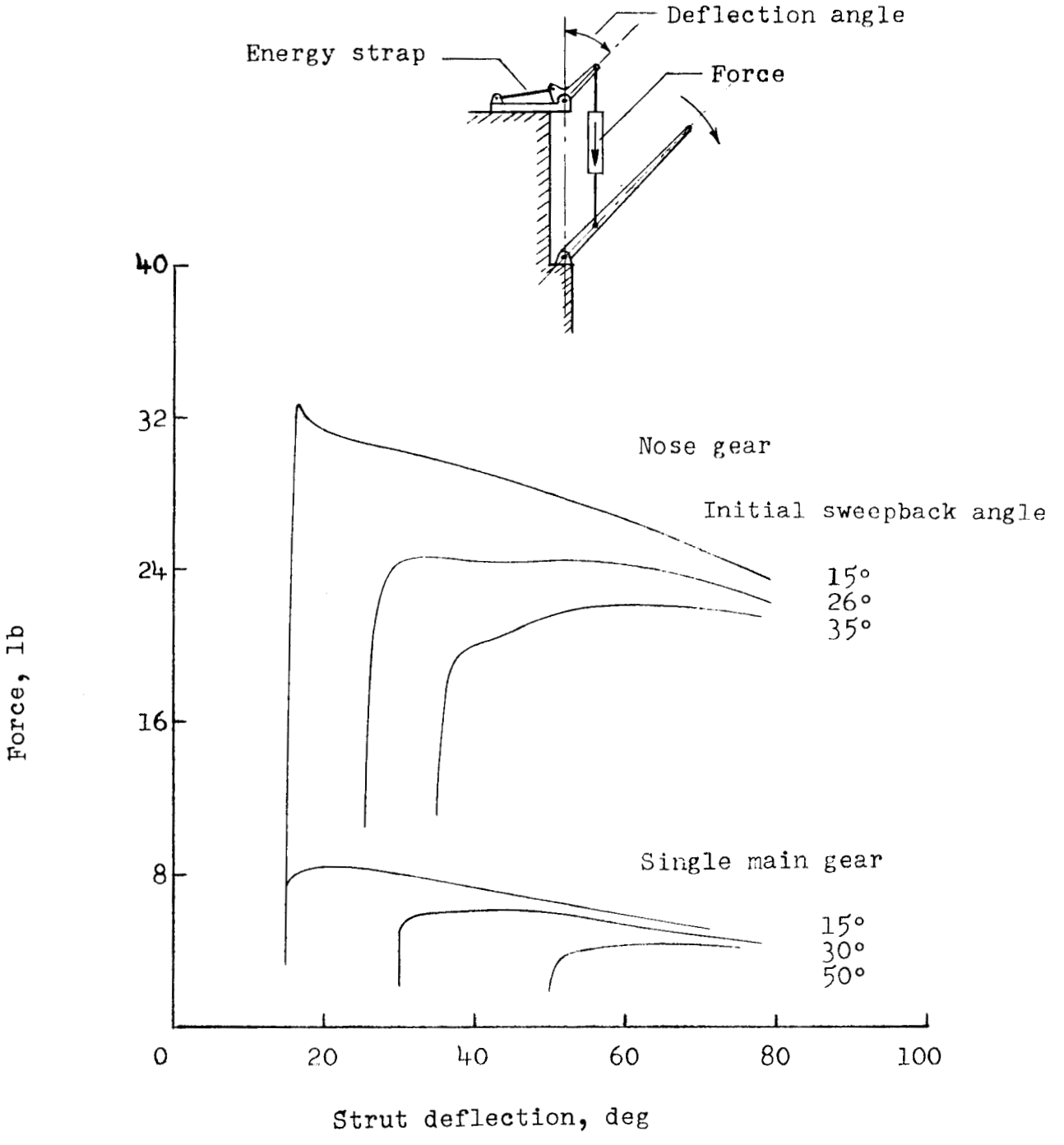

Figure 7.- Typical force-deflection characteristics obtained during component tests of model landing-gear assemblies for various initial strut sweepback angles. Modified gear.

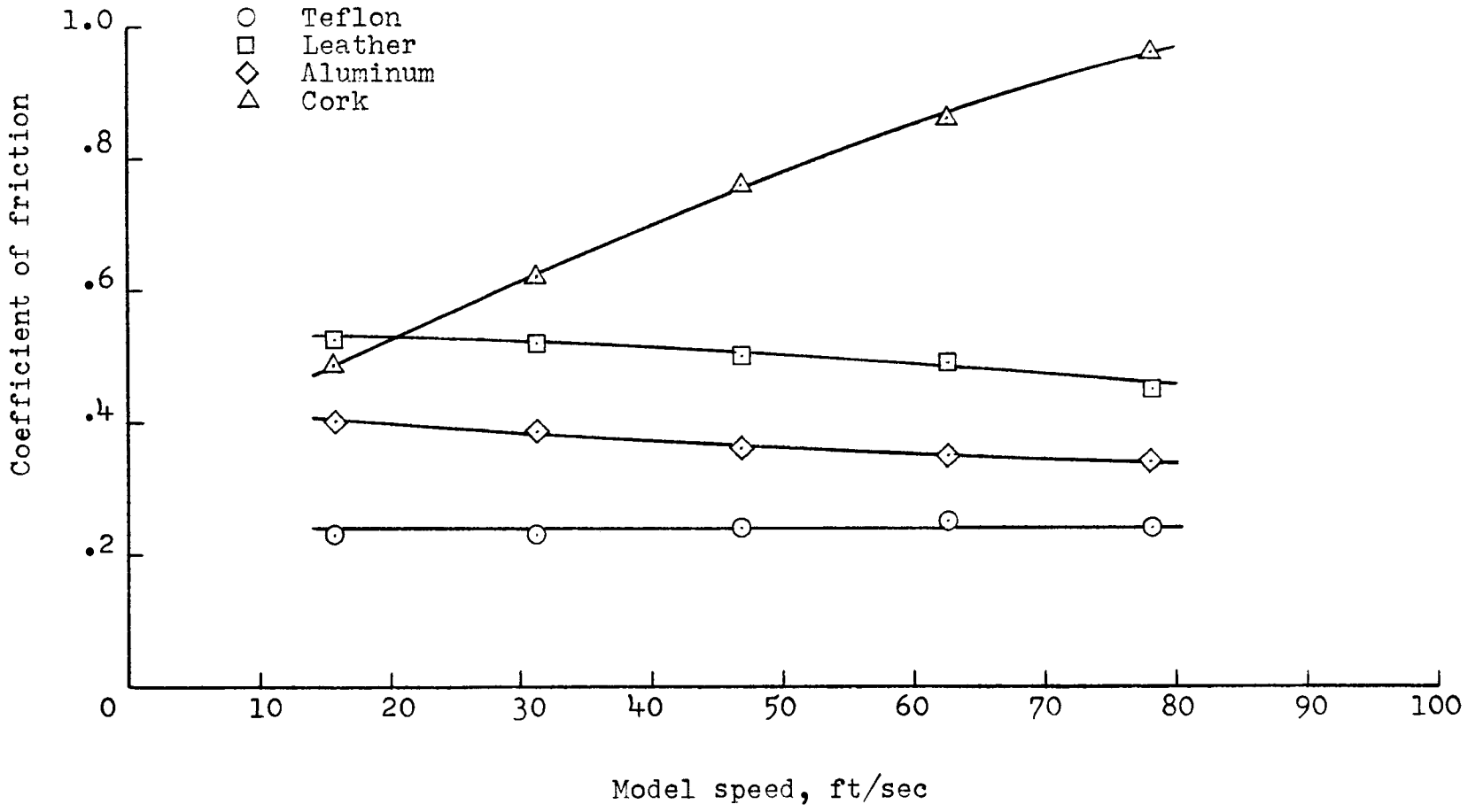

Figure 8.- Approximate coefficient of friction developed by the model skid surfaces sliding on plywood during component test.

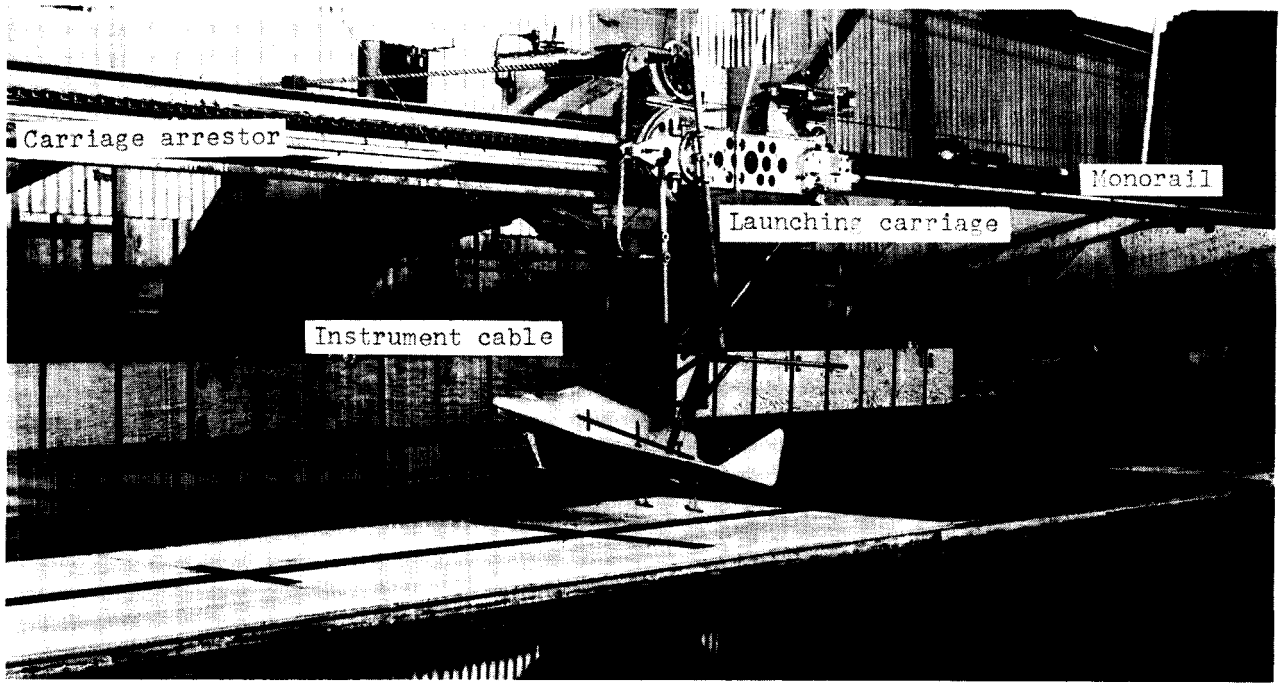

(a) Model and launching gear. L-60-4633.1

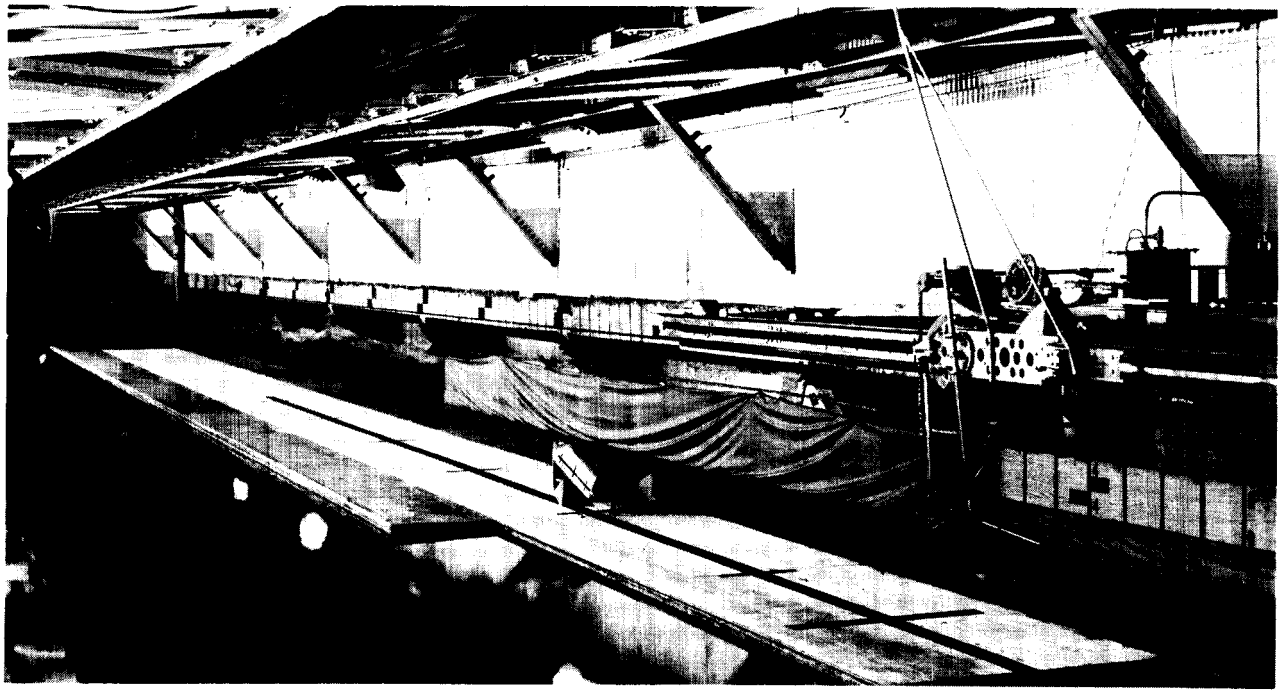

(b) General view of monorail and runway. L-60-4634

Figure 9.- Model on launching gear and landing on runway.

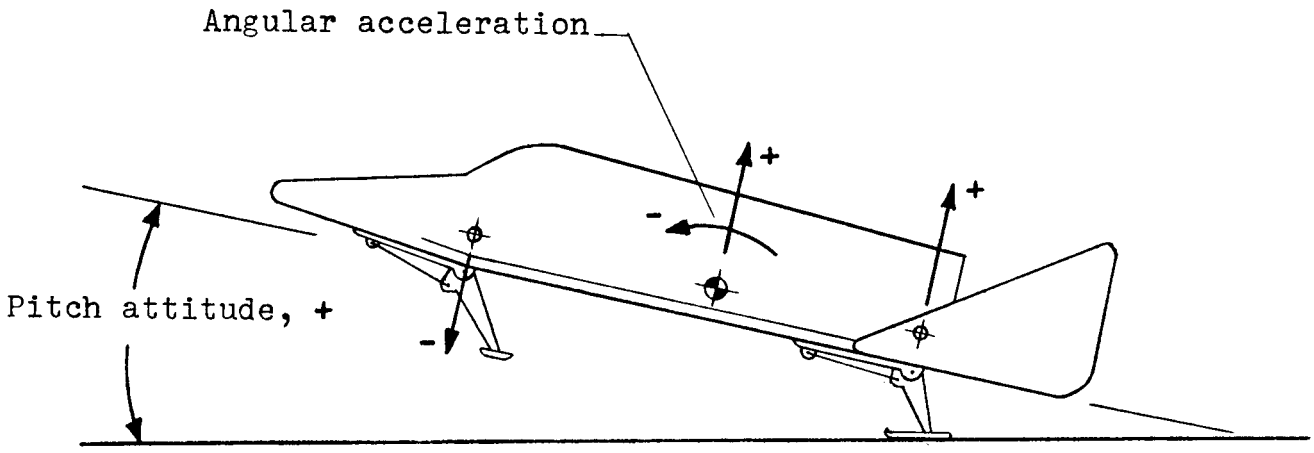

First main-gear impact

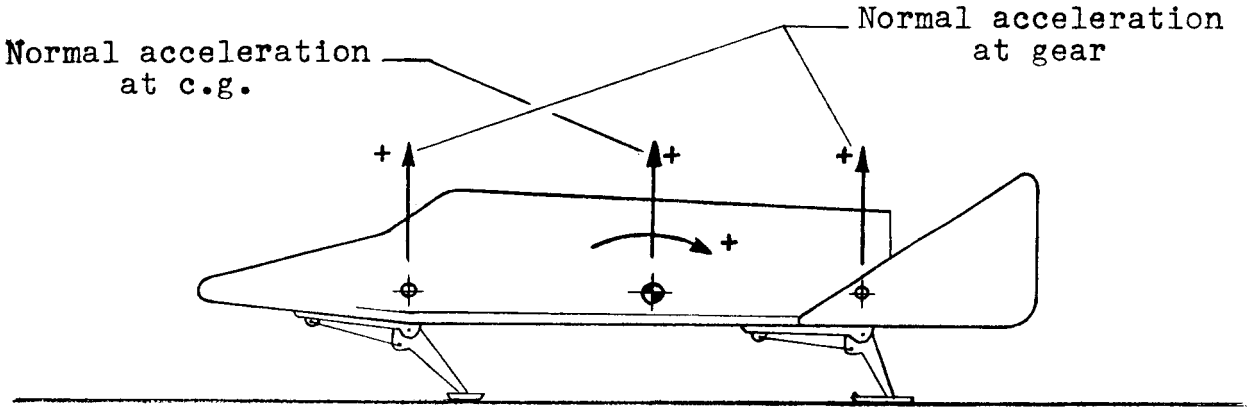

First nose-gear impact

Figure 10.- Sketches identifying acceleration axes and attitude during principal landing impacts.

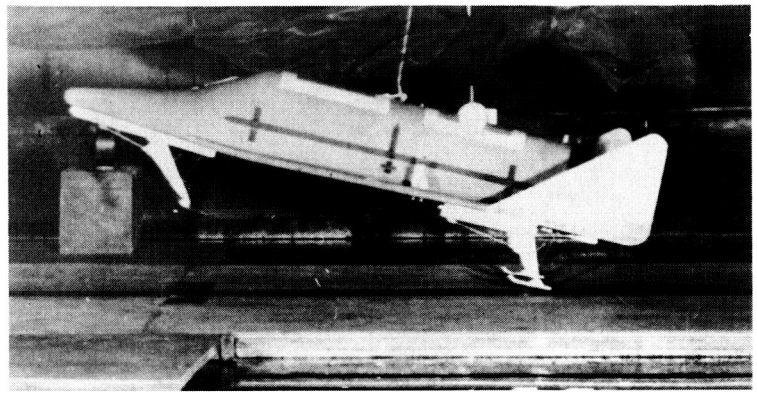

1

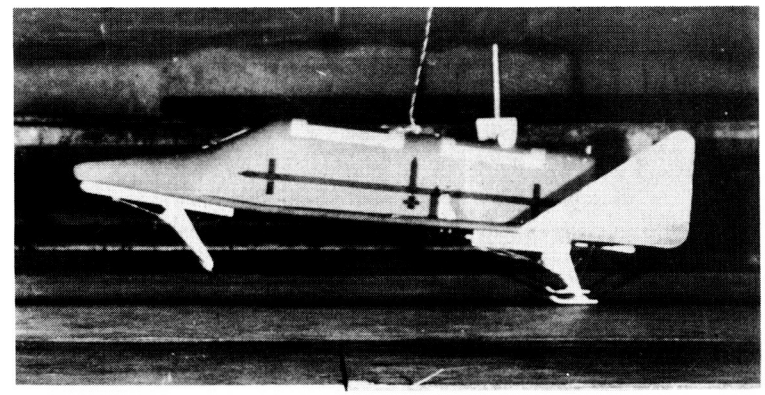

2

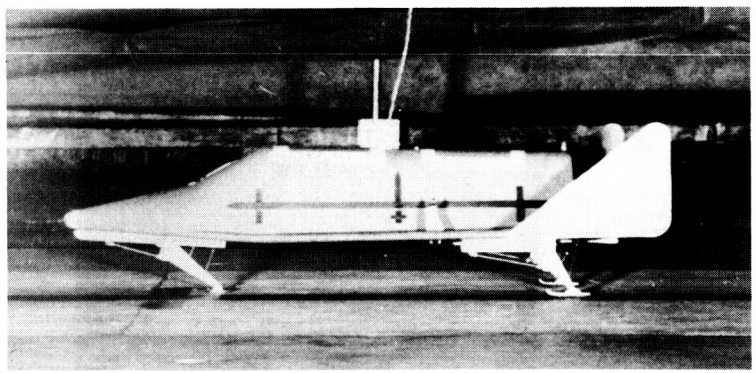

3

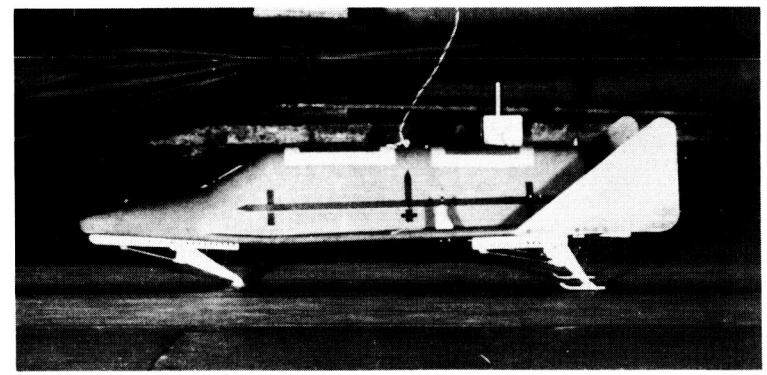

4

L-60-7693

Figure 11.- Sequence photographs during typical landing of model on hard-surface runway.

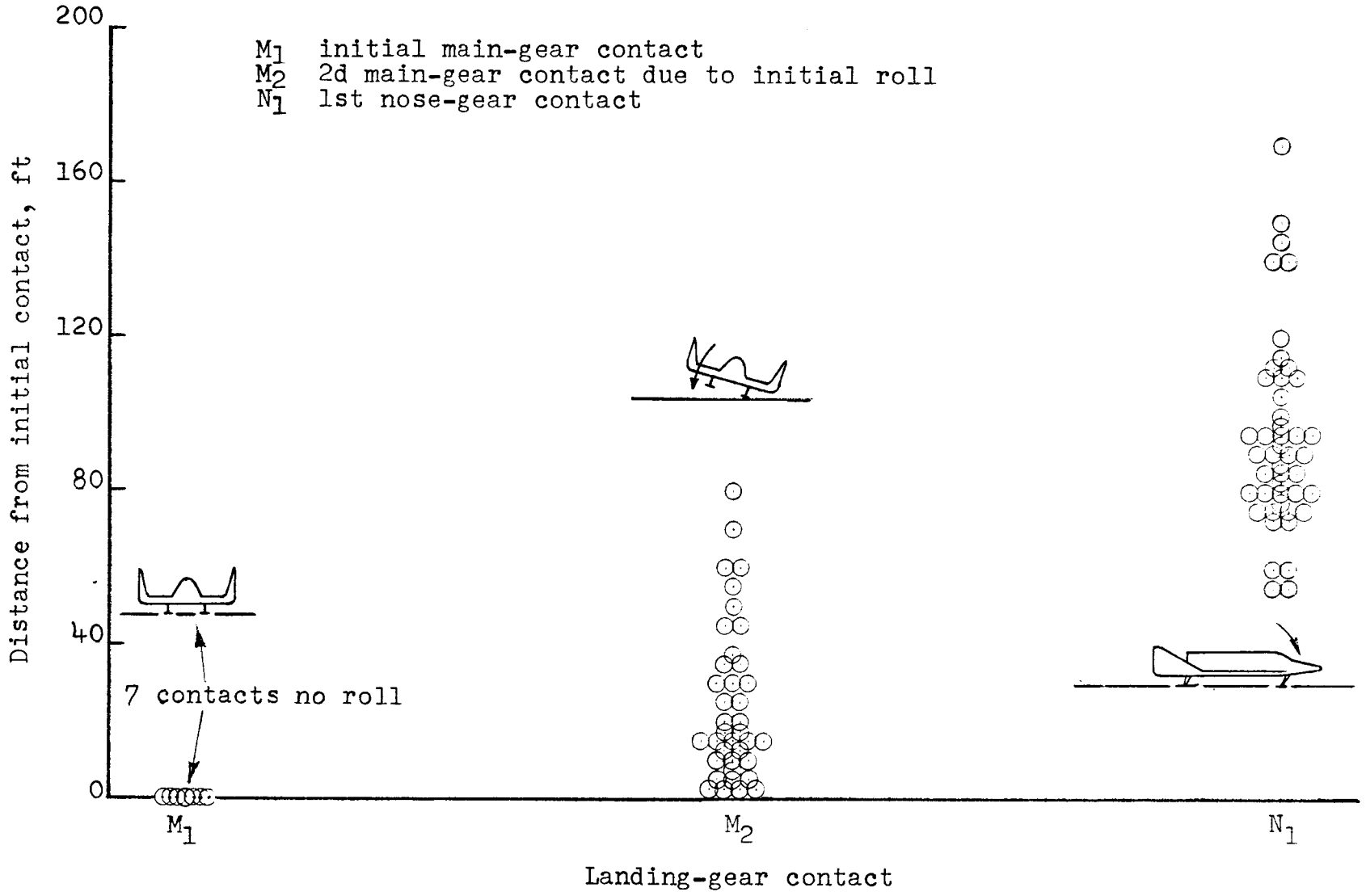

Figure 12.- Landing-gear contact dispersion along slideout path during 46 landings. Touchdown pitch attitude, 15°; gross weight, 8,000 lb; landing speed, 105 knots; initial sinking speed, 4 to 12 ft/sec. All values are full scale.

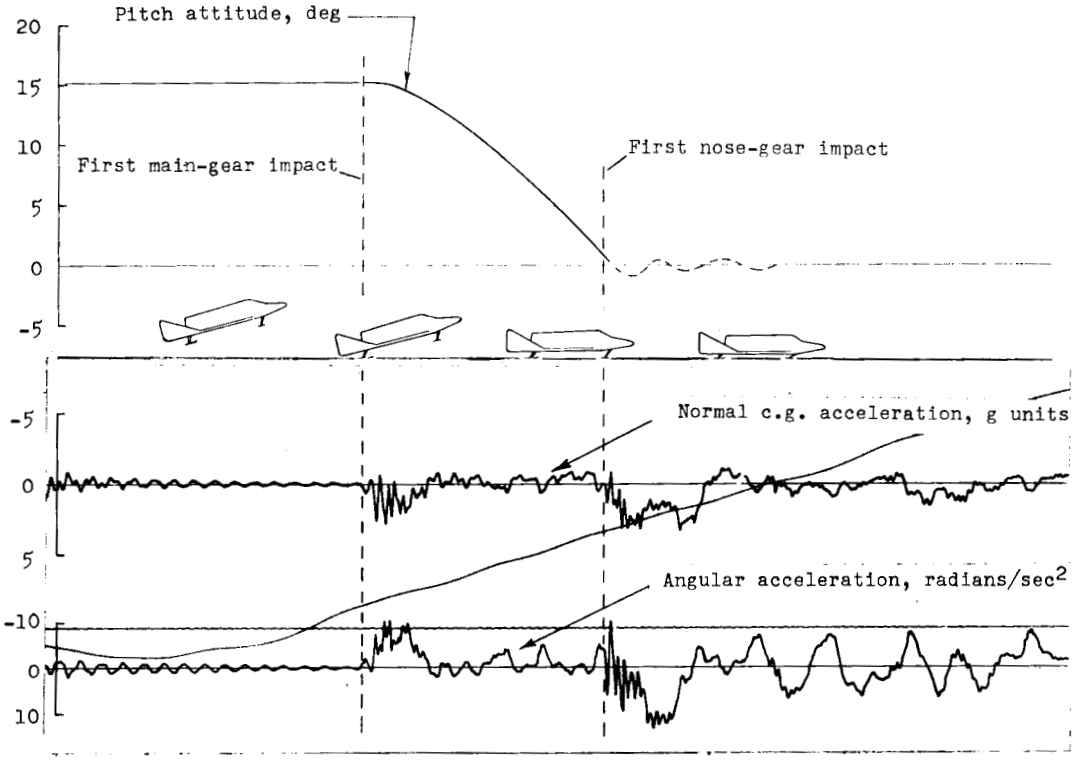

(a) Center-of-gravity accelerations.

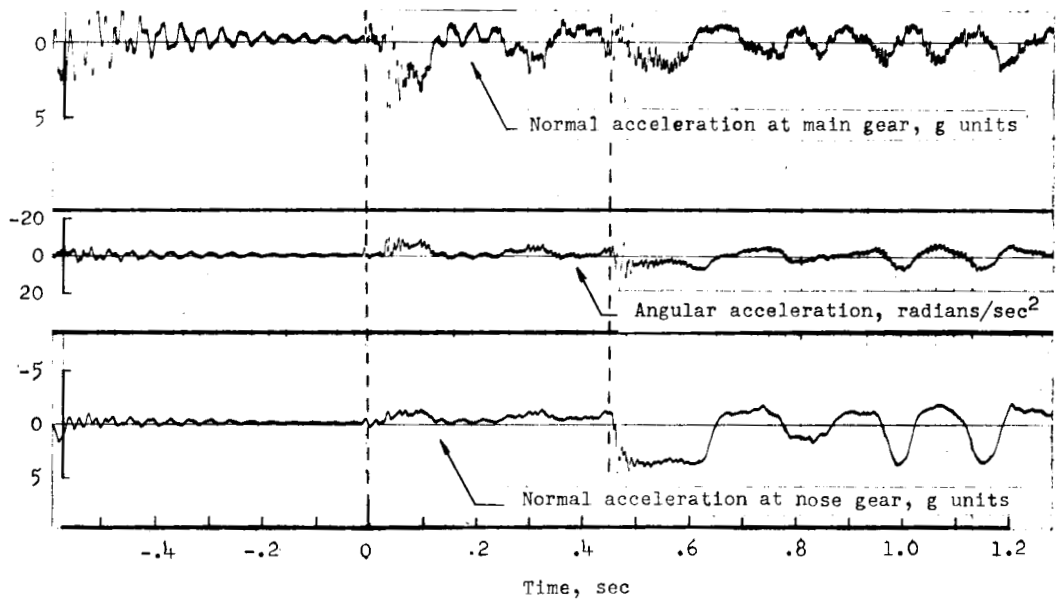

(b) Gear accelerations.

Figure 13.- Typical pitch-acceleration time histories during landings. All values are full scale.

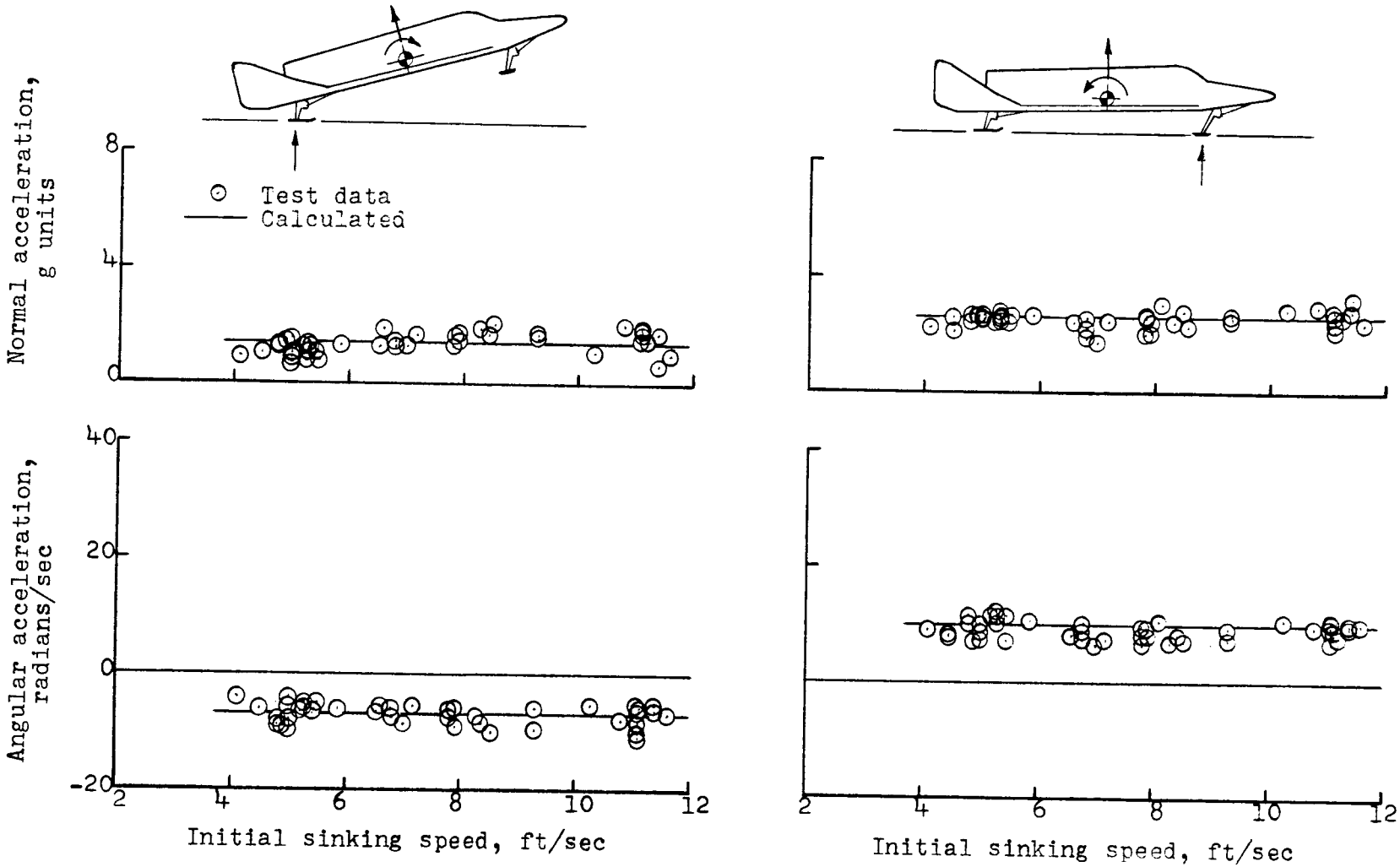

(a) First main-gear impact.

(b) First nose-gear impact.

Figure 14.- Maximum center-of-gravity accelerations at first main- and nose-gear impacts obtained during landings for various initial (touchdown) sinking speeds. Basic gear; forward nose-gear location; touchdown pitch attitude, 15°; gross weight, 8,000 lb; landing speed, 105 knots.

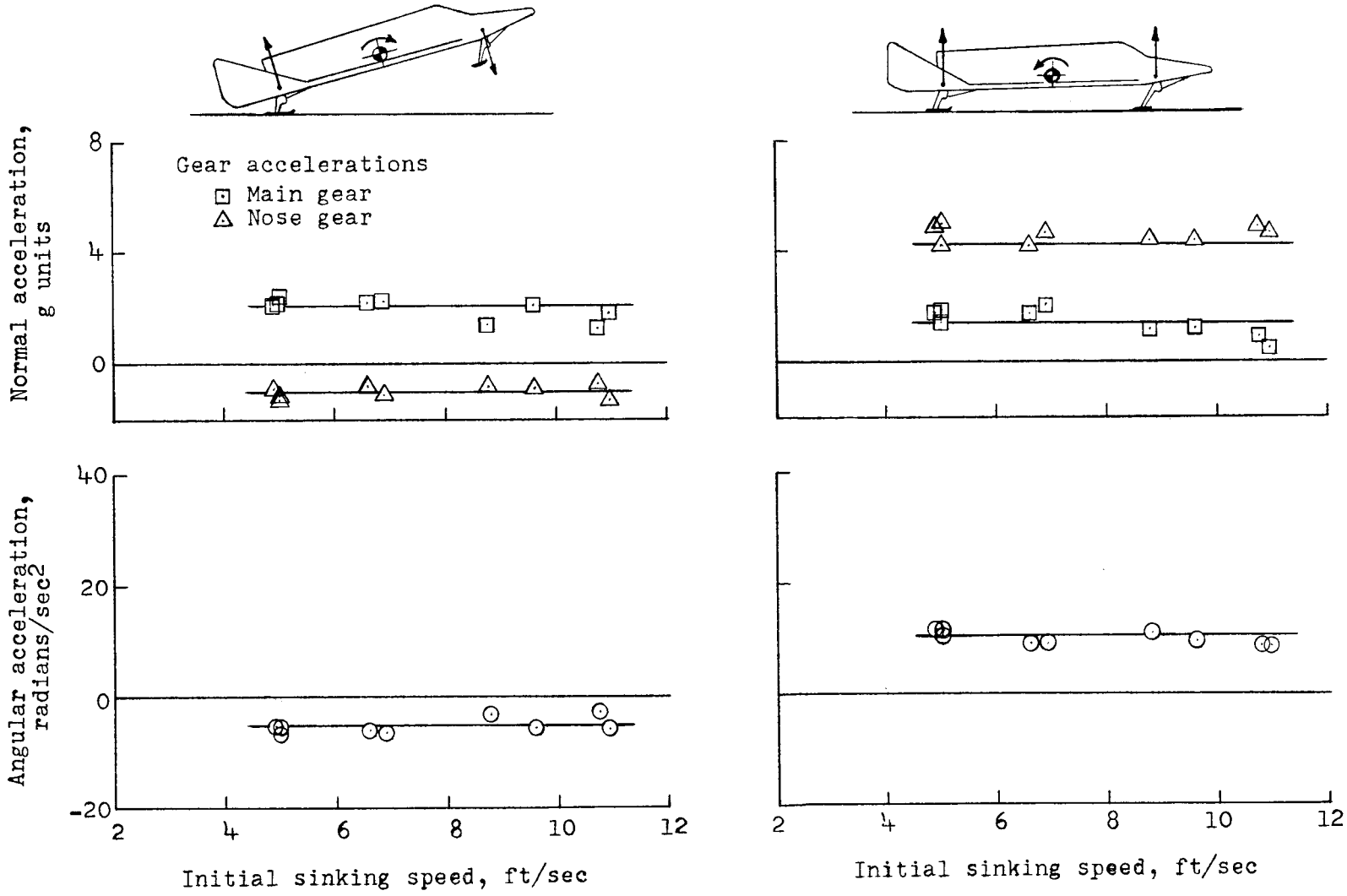

(a) First main-gear impact.

(b) First nose-gear impact.

Figure 15.- Maximum gear accelerations at first main- and nose-gear impacts obtained during landings for various initial (touchdown) sinking speeds. Modified gear; intermediate nose-gear location; touchdown pitch attitude, 15°; gross weight, 8,500 lb; landing speed,

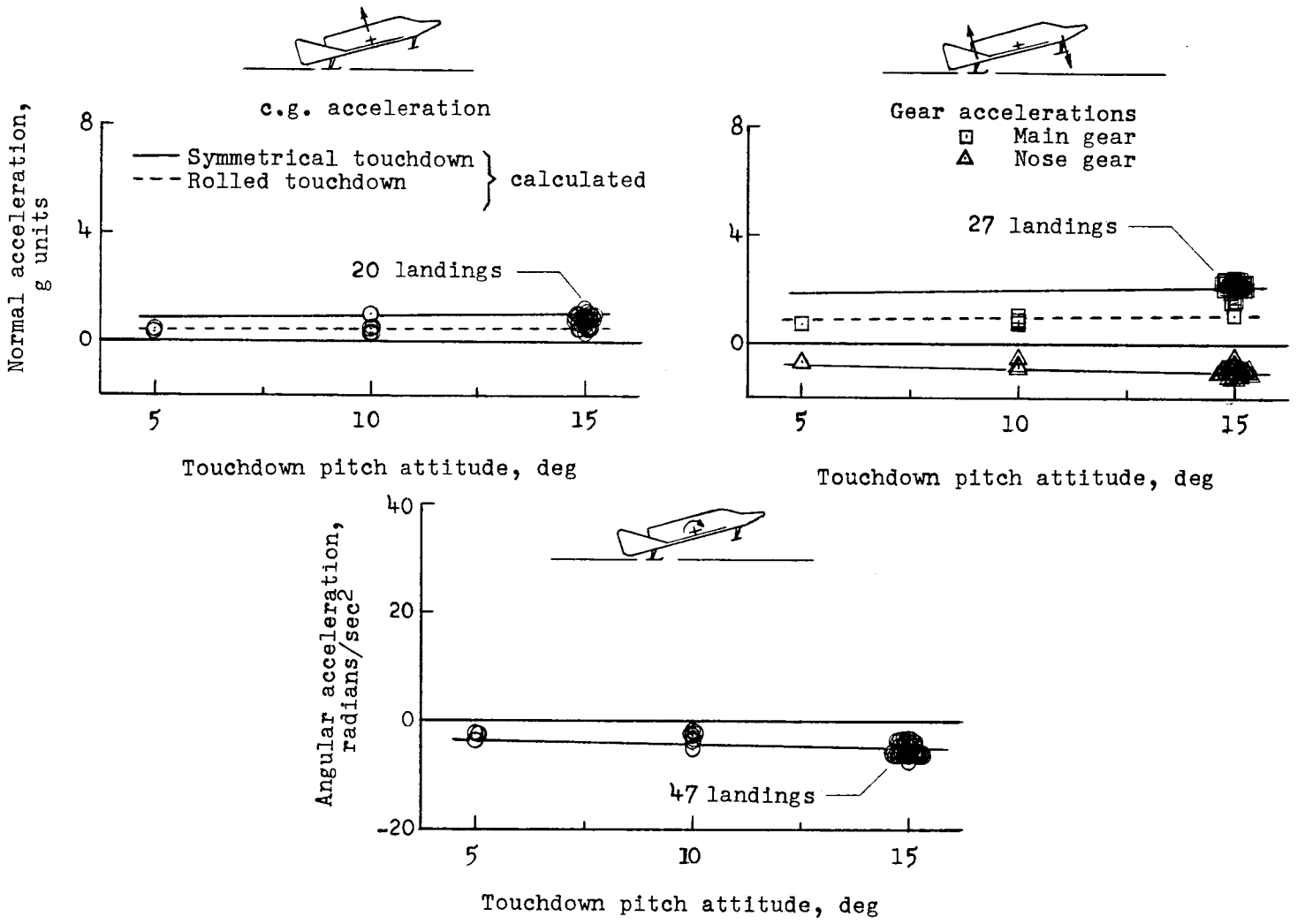

(a) First main-gear impact.

Figure 16.- Maximum accelerations at first main- and nose-gear impacts obtained during landings for various touchdown pitch attitudes. Modified gear; intermediate nose-gear location; gross weight, 8,500 lb; landing speed, 170 knots at 5°, 140 knots at 10°, and 110 knots at 15°.

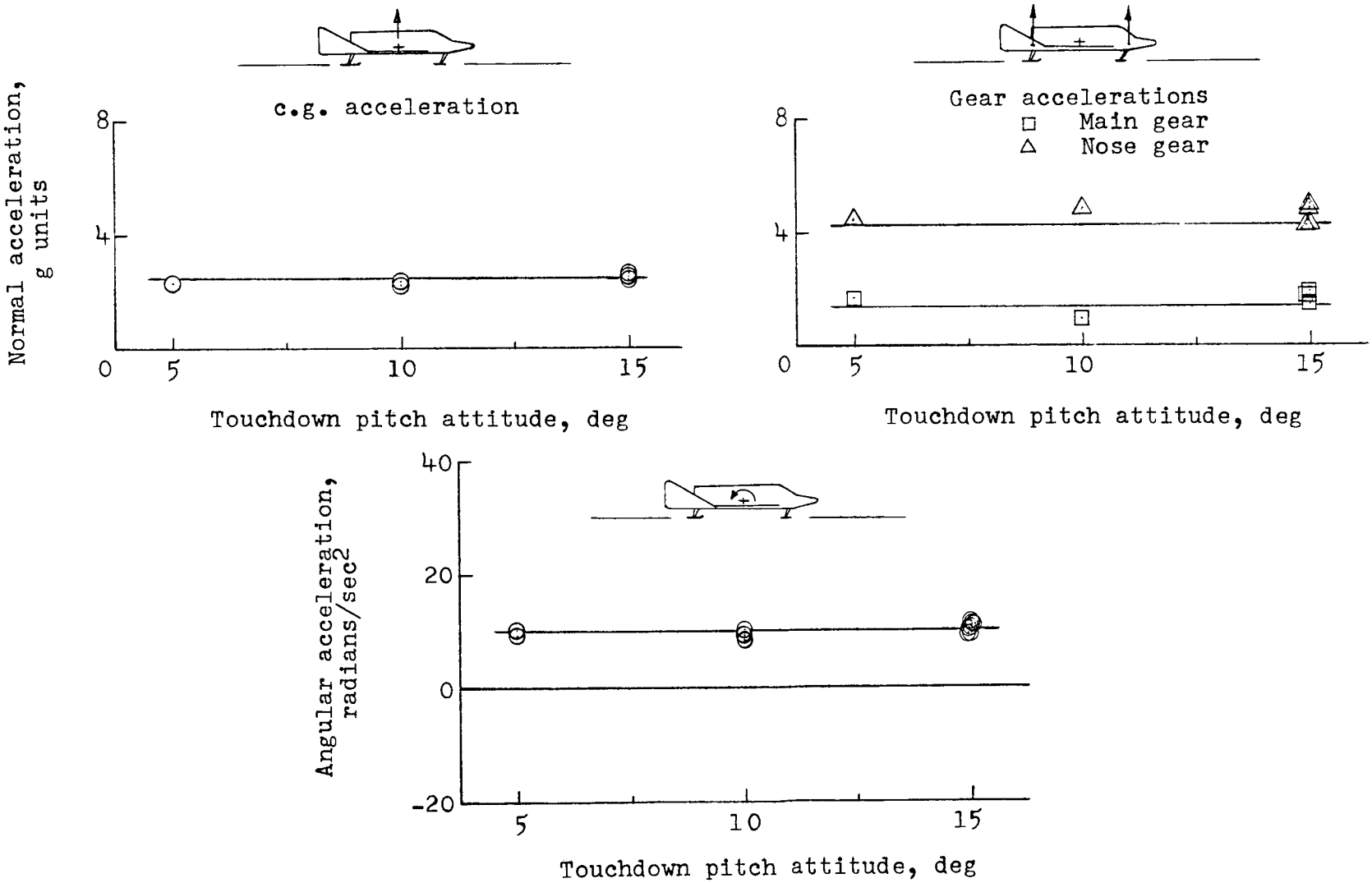

(b) First nose-gear impact.

Figure 16.- Concluded.

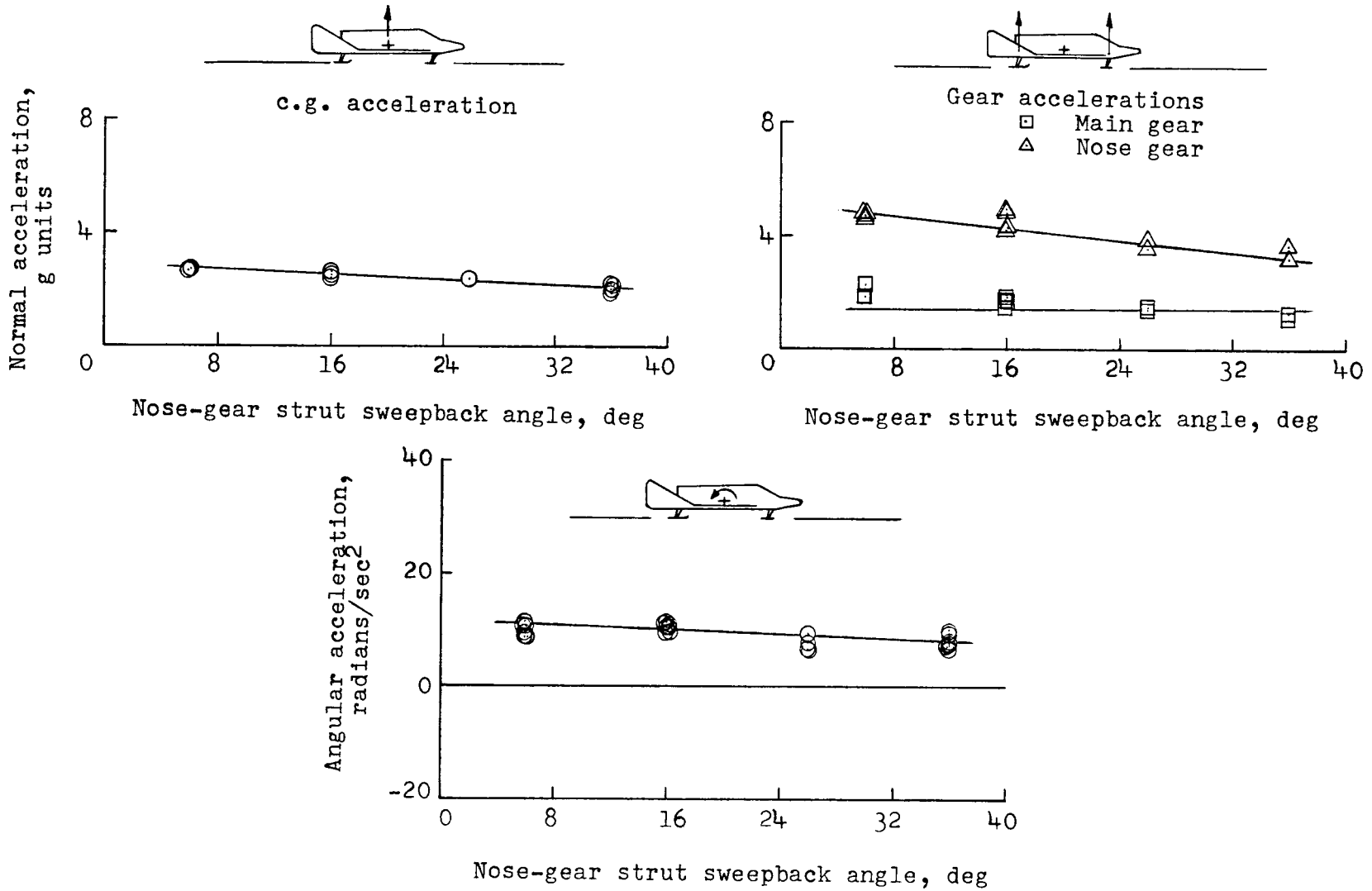

Figure 17.- Maximum accelerations at first nose-gear impact obtained during landings for various initial nose-gear strut sweepback angles. Modified gear; intermediate nose-gear location; gross weight, 8,500 lb; touchdown pitch attitude, 15°; landing speed, 110 knots.

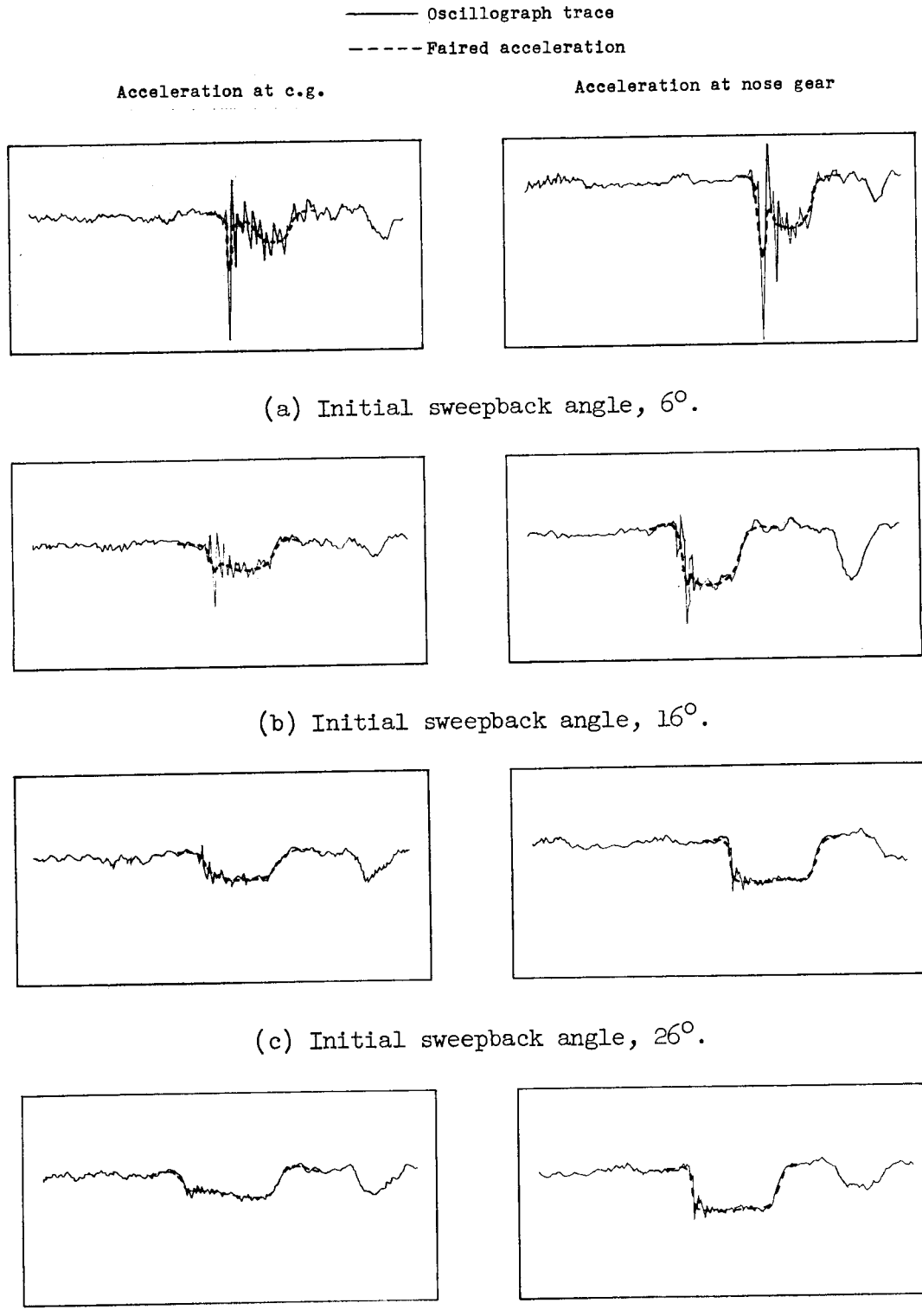

(a) Initial sweepback angle, 6°.

(b) Initial sweepback angle, 16°.

(c) Initial sweepback angle, 26°.

(d) Initial sweepback angle, 36°.

Figure 18.- Typical fairings of traces of normal acceleration at first nose-gear impact obtained during landings for various initial nose-gear strut sweepback angles.

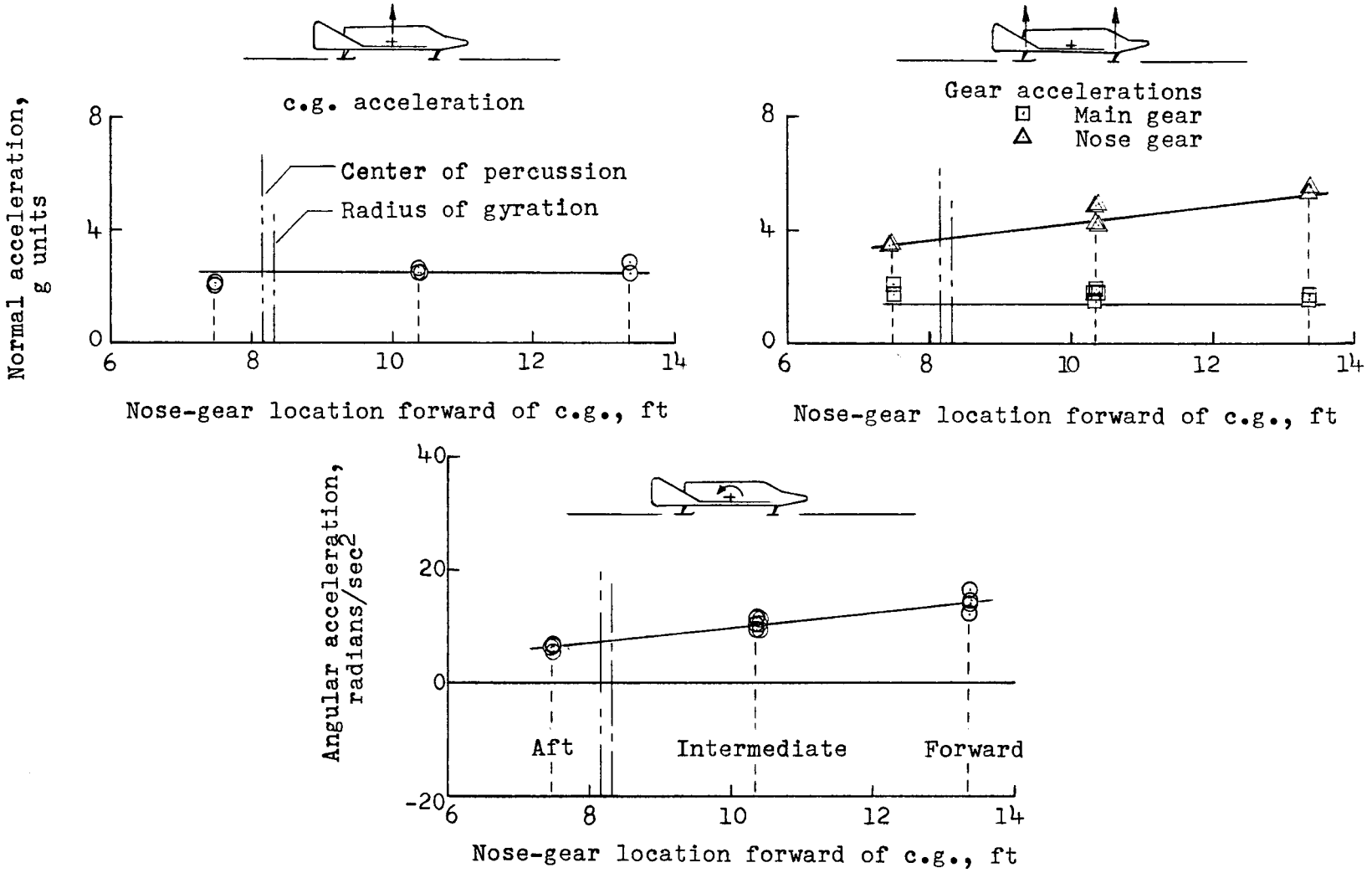

(a) Nose-gear strut sweepback, 16°.

Figure 19.- Maximum accelerations at first nose-gear impact obtained during landings for the nose-gear locations. Modified gear; gross weight, 8,500 lb; touchdown pitch attitude, 15°; landing speed, 110 knots.

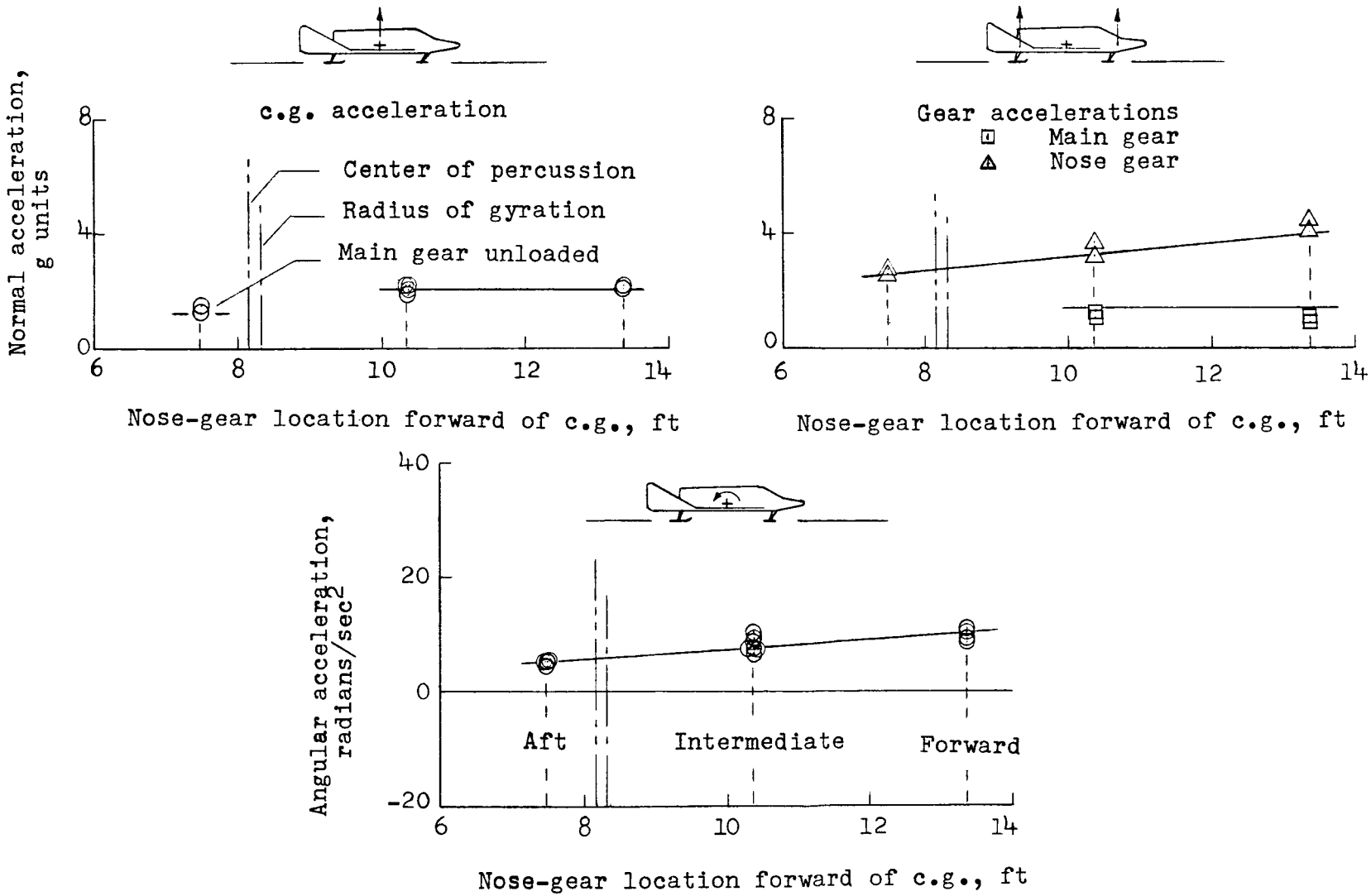

(b) Nose-gear strut sweepback, 36°.

Figure 19.- Concluded.

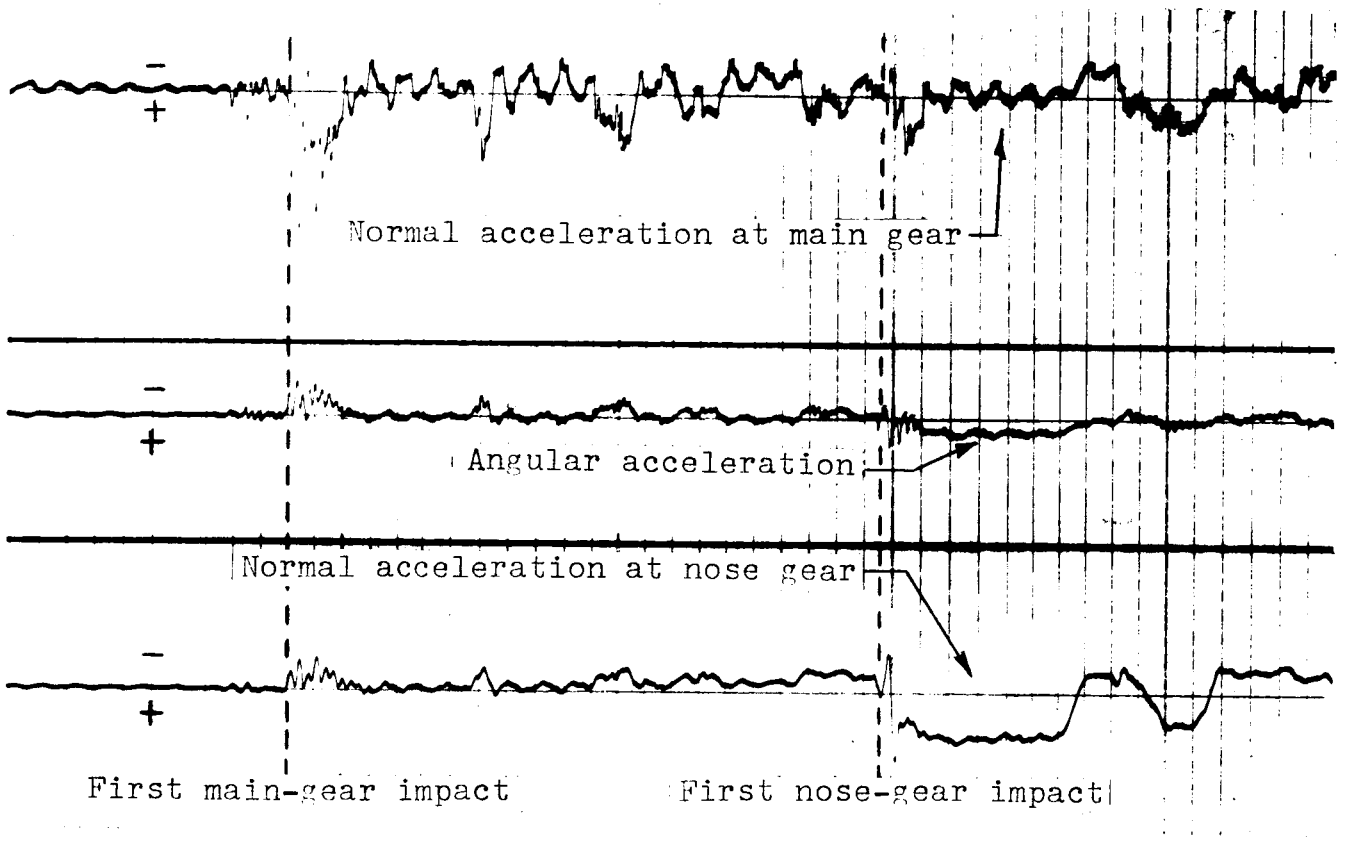

Figure 20.- Oscillograph record of accelerations during landing with nose gear in aft location. Modified gear; nose-gear strut sweepback angle, 36°.

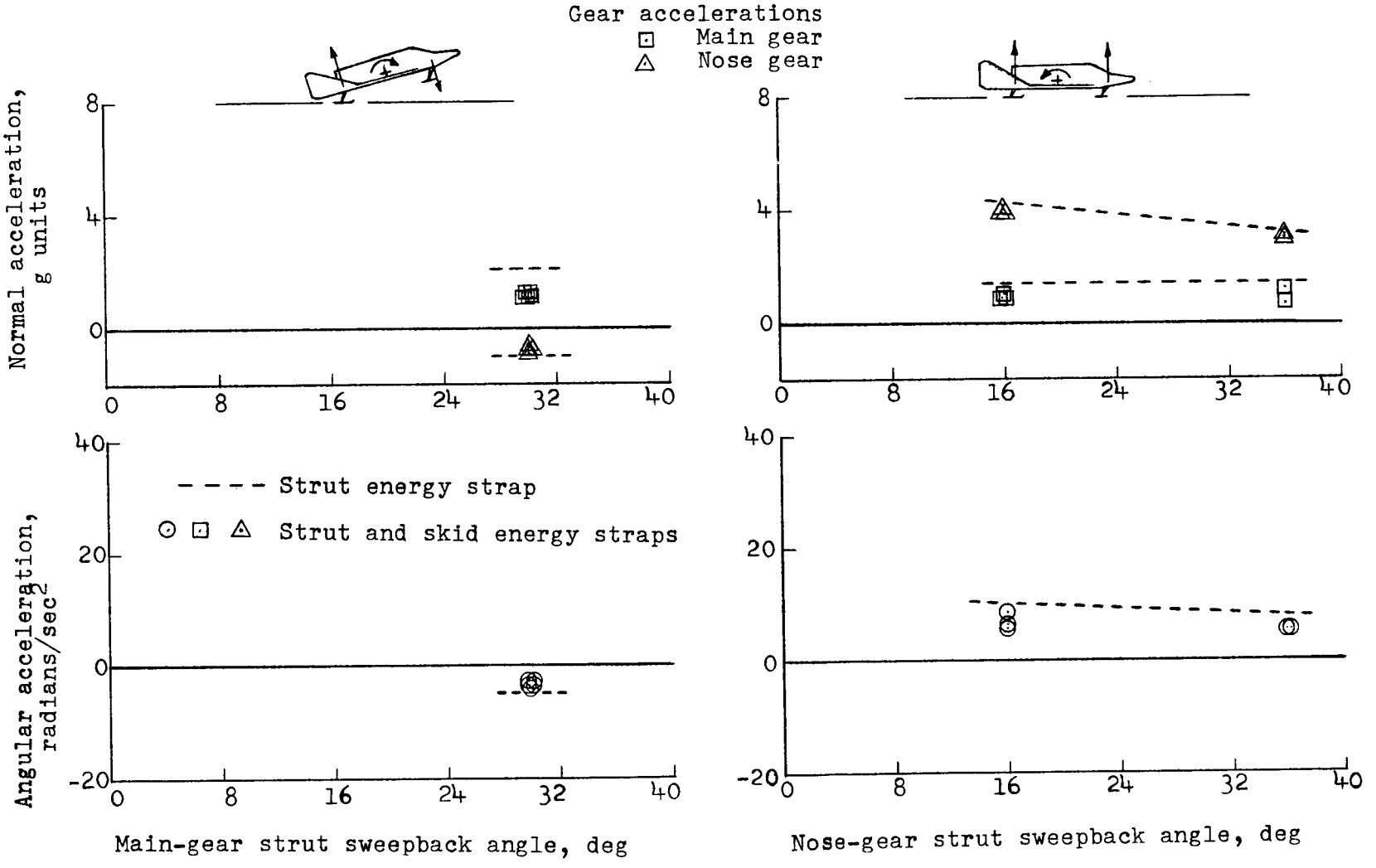

(a) First main-gear impact.

(b) First nose-gear impact.

Figure 21.- Effect of auxiliary skid energy strap on maximum accelerations at first main- and nose-gear impacts obtained during landings for various initial strut sweepback angles. Modified gear; intermediate nose-gear location; gross weight, 8,500 lb; touchdown pitch attitude, 15°; landing speed, 110 knots.

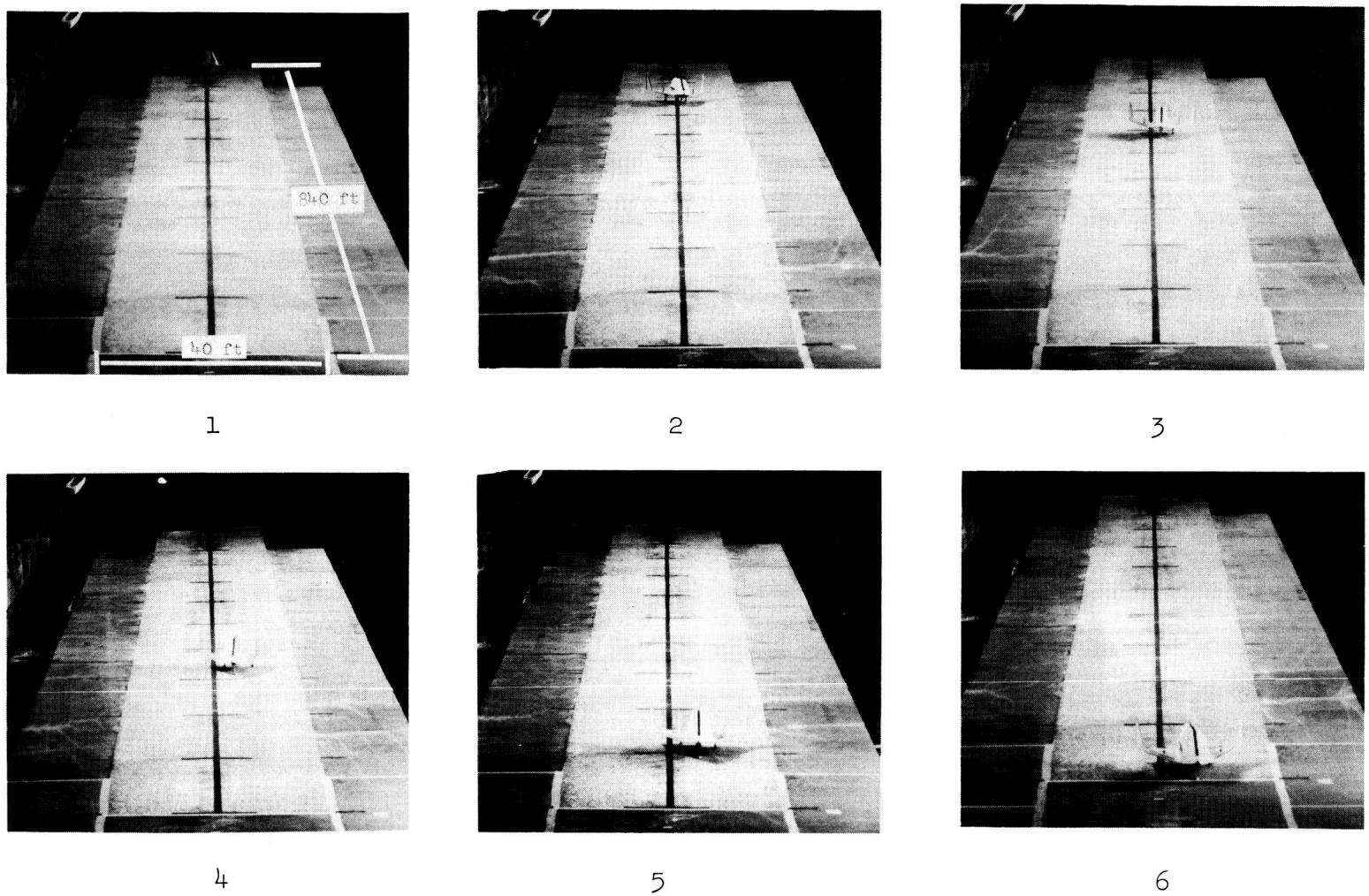

(a) Coefficient-of-friction ratio, 2.0. (Coefficient at main skid, 0.5; coefficient at nose skid, 0.25.) L-62-2129

Figure 22.- Sequence photographs obtained during yawed slideout tests showing effect of ratio of main- to nose-skid coefficient of friction at a launch speed of 110 knots. Modified gear; intermediate nose-gear location; gross weight, 8,500 lb; pitch attitude, 0°; yaw at launch, 10° left.

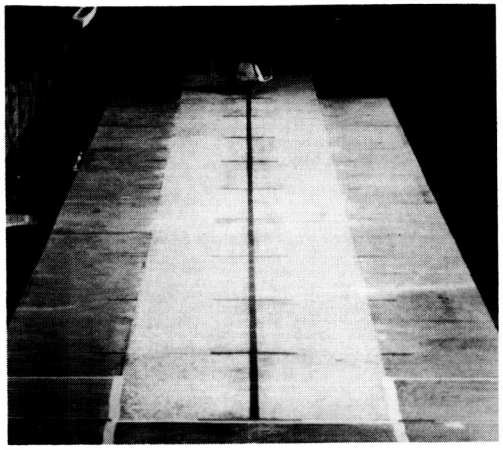

1

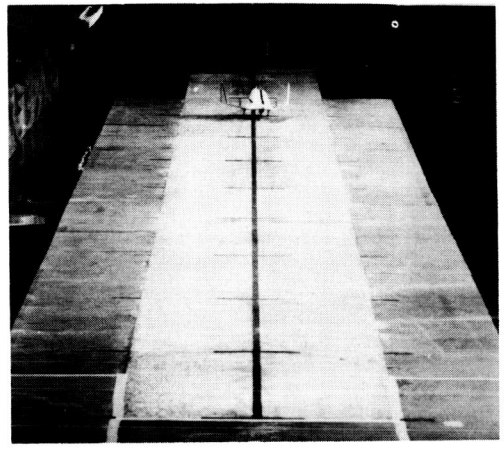

2

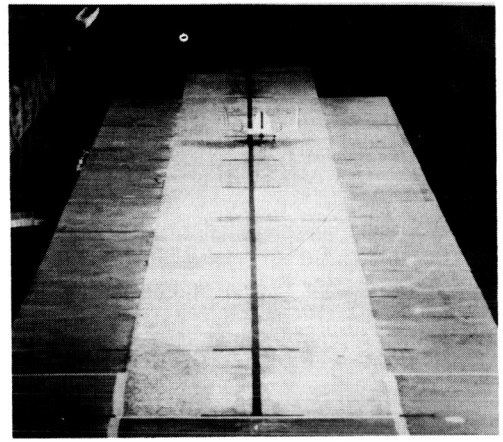

3

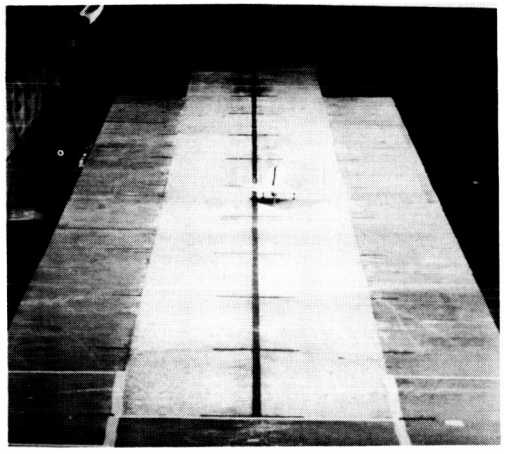

4

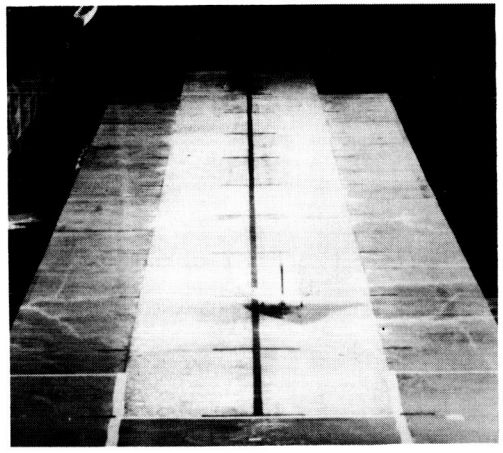

5

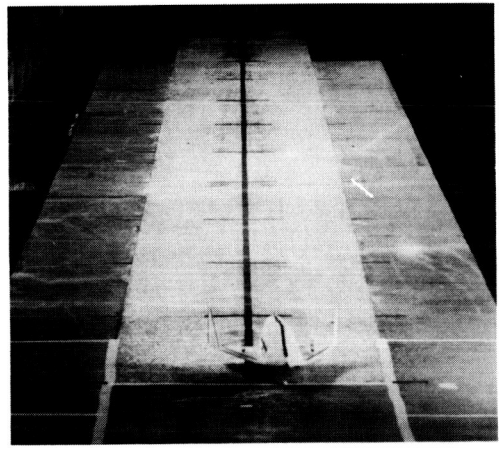

6

(b) Coefficient-of-friction ratio, 1.0. (Coefficient at main skid, 0.25; L-62-2130
coefficient at nose skid, 0.25.)

Figure 22.- Continued.

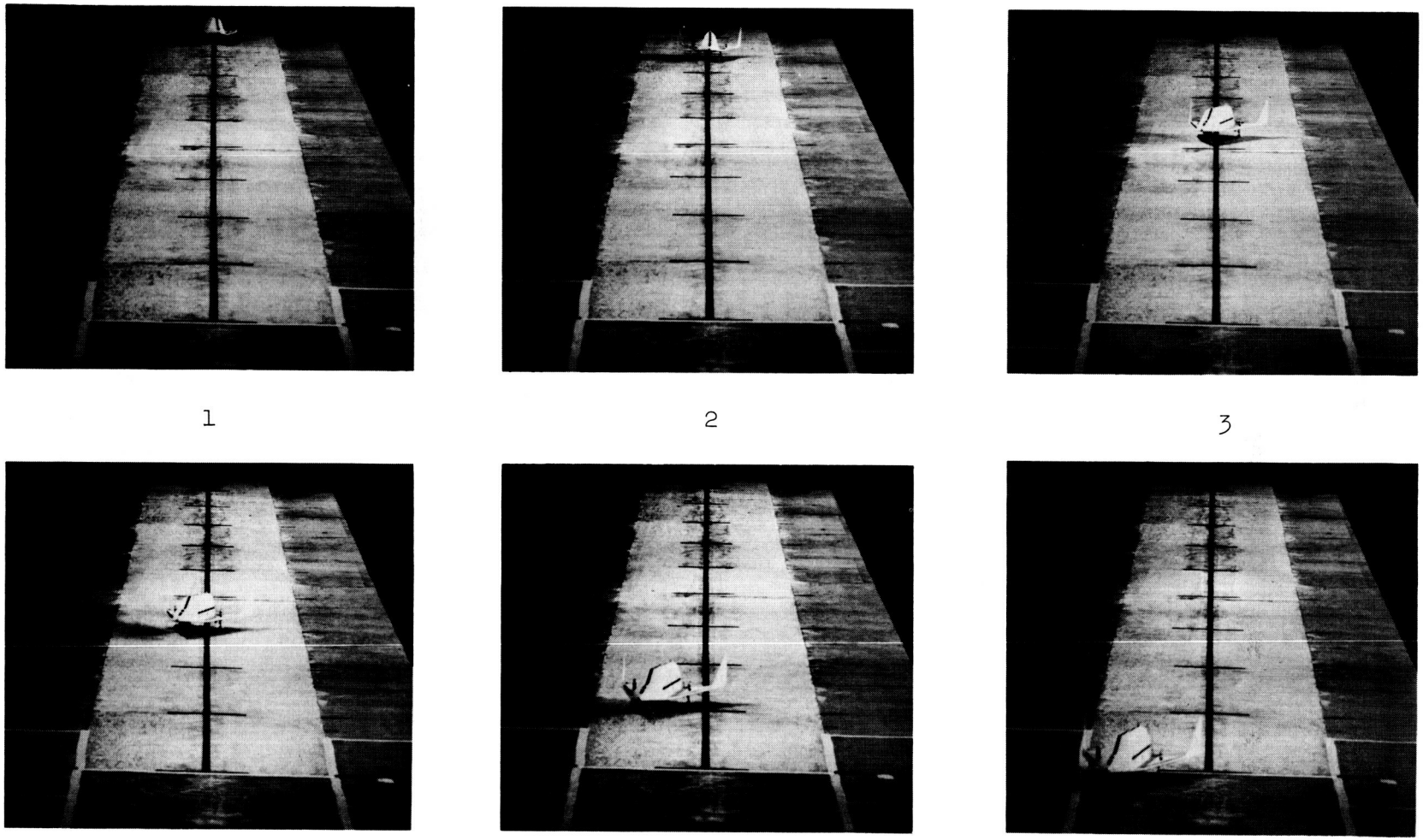

(c) Coefficient-of-friction ratio, 0.6. (Coefficient at main skid, 0.25; coefficient at nose skid, 0.4.) L-62-2131

Figure 22.- Continued.

(d) Coefficient-of-friction ratio, 0.4. (Coefficient at main skid, 0.25; coefficient at nose skid, 0.7.) L-62-2132

Figure 22.- Concluded.

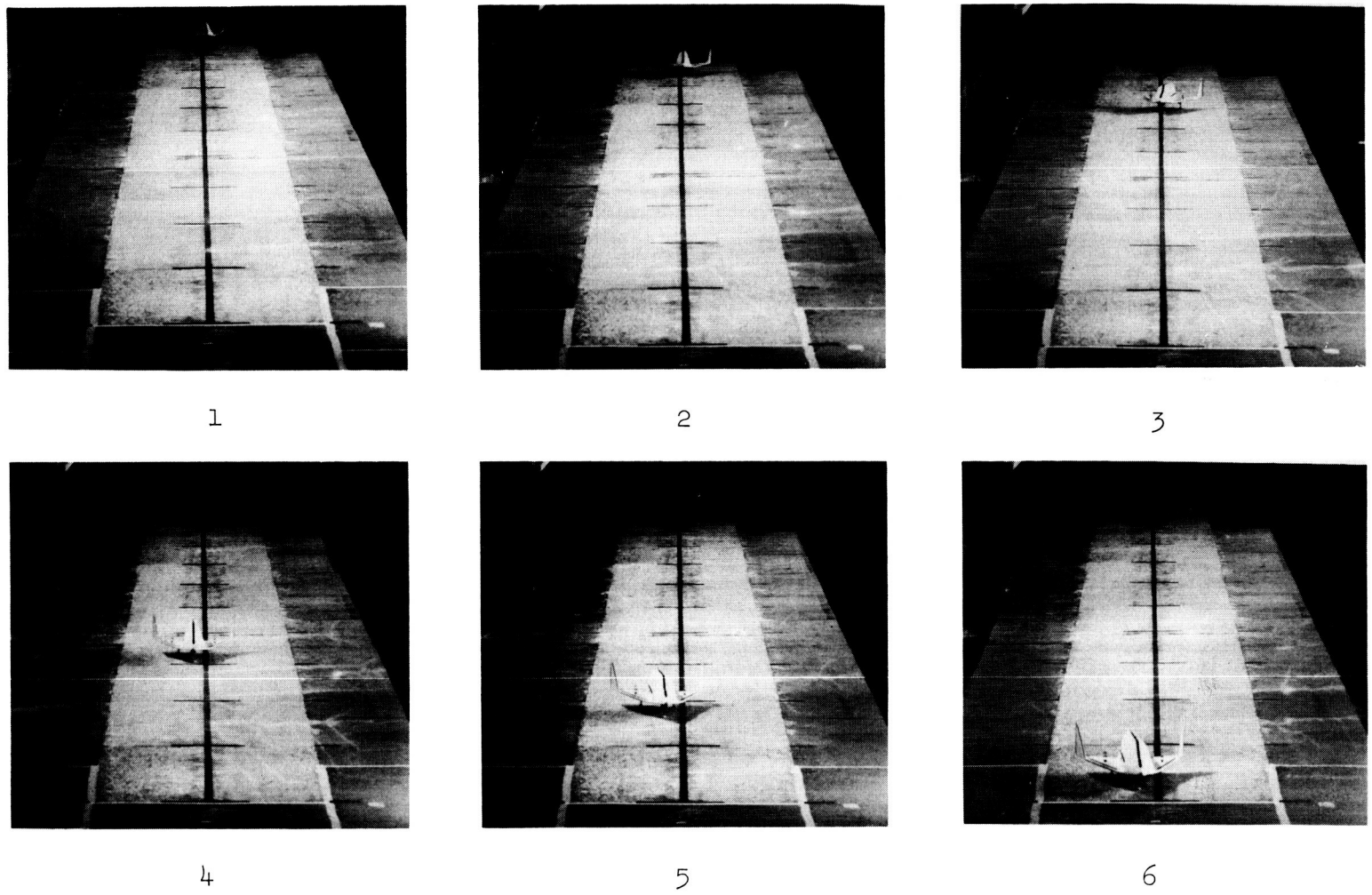

(a) Coefficient-of-friction ratio, 2.0. (Coefficient at main skid, 0.5; coefficient at nose skid, 0.25.) L-62-2133

Figure 23.- Sequence photographs obtained during yawed slideout tests showing effect of ratio of main- to nose-skid coefficient of friction at a launch speed of 75 knots. Modified gear; intermediate nose-gear location; gross weight, 8,500 lb; pitch attitude, 0°; yaw at launch, 10° left.

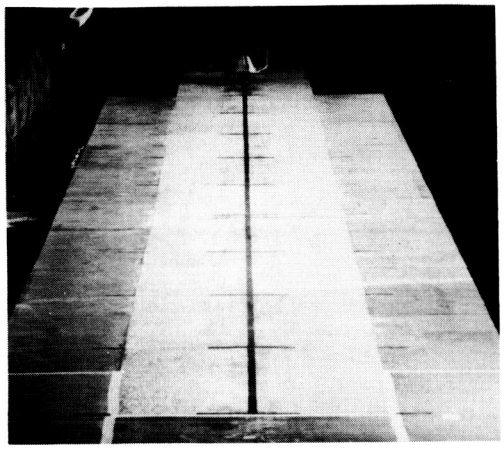

1

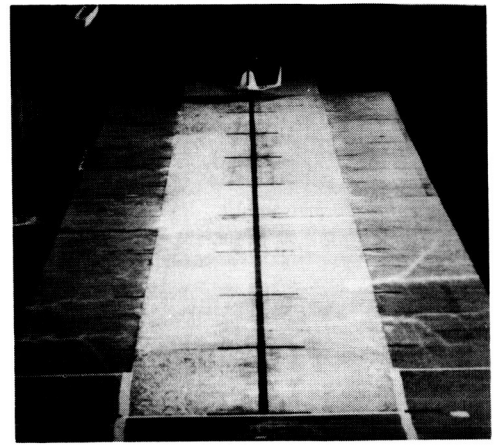

2

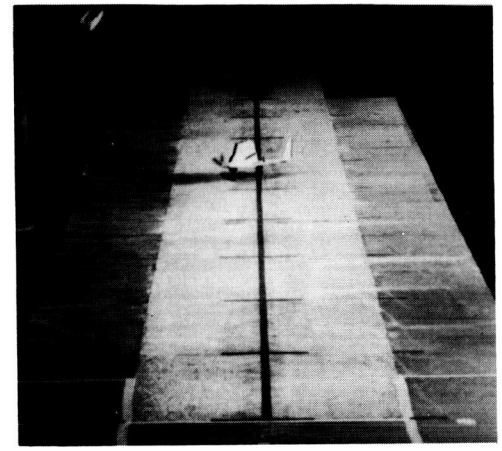

3

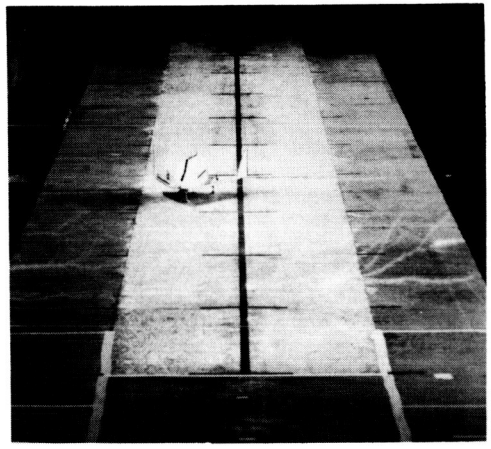

4

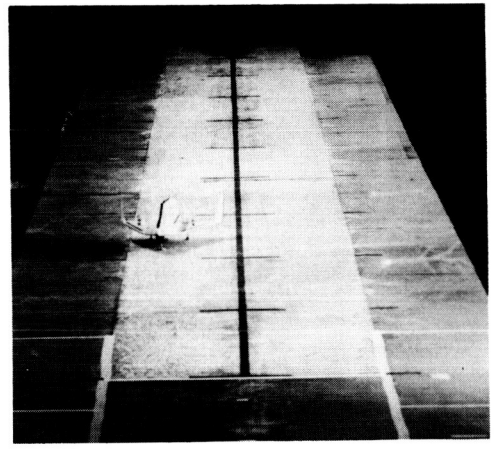

5

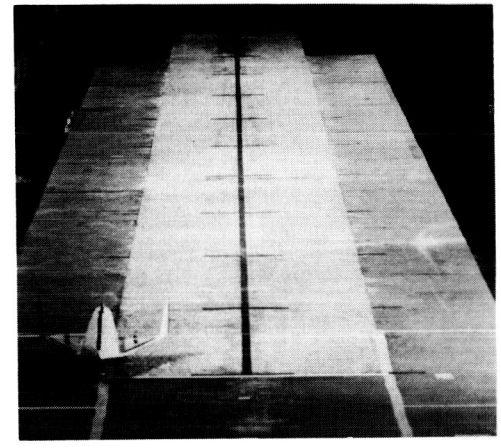

6

(b) Coefficient-of-friction ratio, 1.0. (Coefficient at main skid, 0.25; coefficient at nose skid, 0.25.) L-62-2134

Figure 23.- Continued.

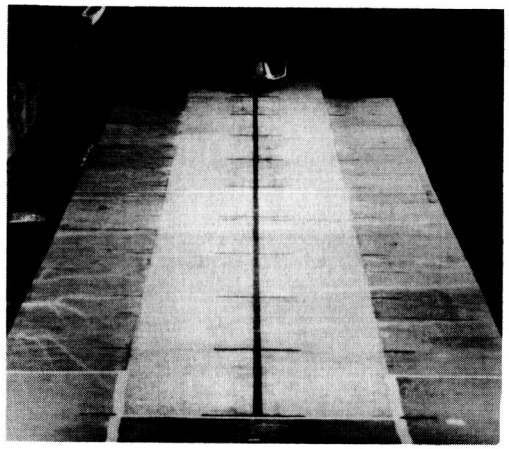

1

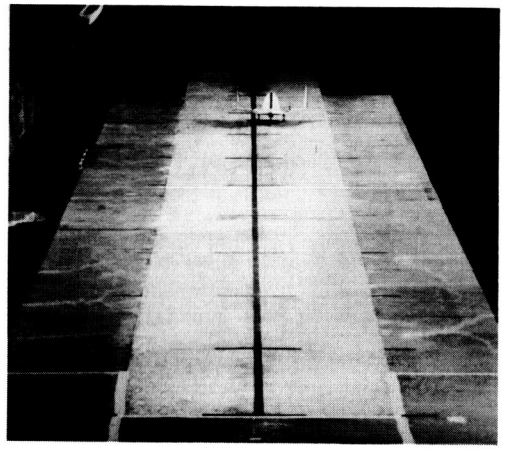

2

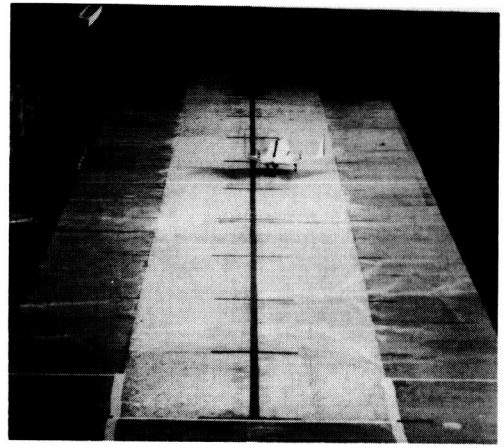

3

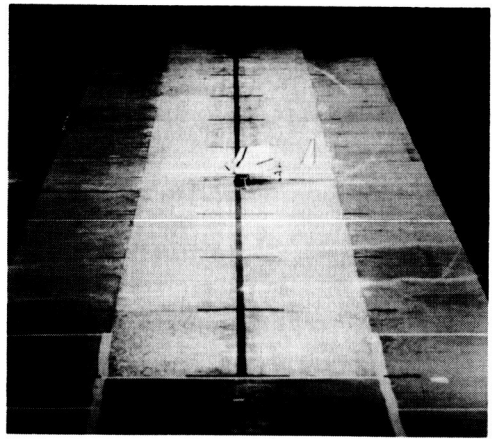

4

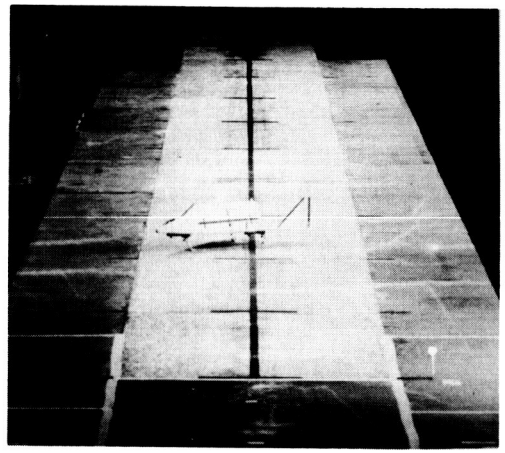

5

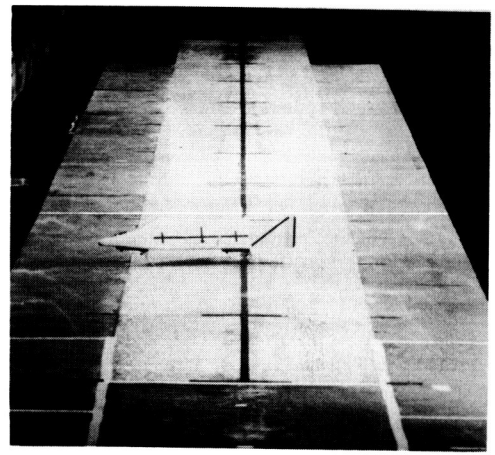

6

(c) Coefficient-of-friction ratio, 0.6. (Coefficient at main skid, 0.25; coefficient at nose skid, 0.4.) L-62-2135

Figure 23.- Continued.

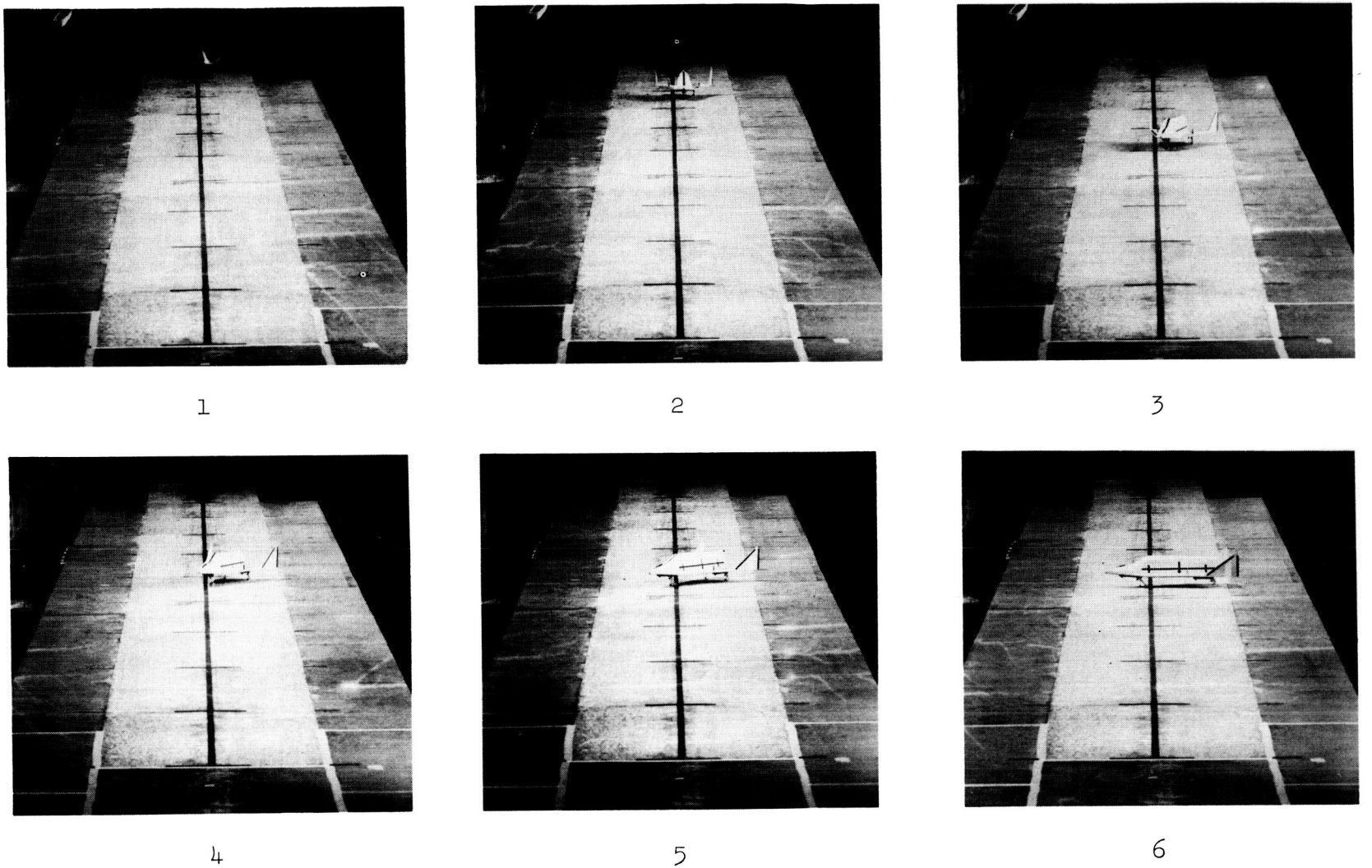

(d) Coefficient-of-friction ratio, 0.4. (Coefficient at main skid, 0.25; coefficient at nose skid, 0.7.)

Figure 23.- Concluded.